

1 **Landsat and Sentinel-derived glacial lake dataset in the China-**
2 **Pakistan Economic Corridor from 1990 to 2020**

3
4 Muchu Lesi¹, Yong Nie^{1, *}, Dan H. Shugar², Jida Wang³, Qian Deng^{1, 4}, Huayong Chen¹,
5 [Jianrong Fan¹](#)

6
7 ¹Institute of Mountain Hazards and Environment, Chinese Academy of Sciences, Chengdu,
8 China.

9 ²Water, Sediment, Hazards, and Earth-surface Dynamics (waterSHED) Lab, Department of
10 Geoscience, University of Calgary, Alberta, T2N 1N4, Canada

11 ³Department of Geography and Geospatial Sciences, Kansas State University, Manhattan,
12 Kansas 66506, USA

13 ⁴University of Chinese Academy of Sciences, Beijing 100190, China

14
15
16
17 *Corresponding author, nieyong@imde.ac.cn
18
19

20 **Abstract.** The China-Pakistan Economic Corridor (CPEC) is one of the flagship projects of
21 the One Belt One Road Initiative, which faces threats from water shortage and mountain
22 disasters in the high-elevation ~~-altitude~~ region, such as glacial lake outburst floods (GLOFs).
23 An up-to-date high-quality glacial lake dataset with parameters such as lake area, volume and
24 lake type, ~~acquisition date and area,~~ which is fundamental to water resource and flood risk
25 assessments, and predicting glacier-lake evolutions ~~and cryosphere hydrological interactions,~~
26 is still largely absent for the entire CPEC. This study describes a glacial lake dataset for the
27 CPEC, ~~based on using an~~ threshold-based ~~object-oriented~~ mapping method associated with
28 rigorous visual inspection workflows. This dataset includes (1) multi-temporal inventories for
29 1990, 2000, and 2020 produced from 30 m resolution Landsat images ~~a glacial lake inventory~~
30 ~~for the year 2020 at 10 m resolution produced from Sentinel spectral images,~~ and (2) a glacial
31 lake inventory for the year 2020 at 10 m resolution produced from Sentinel-2 ~~spectral images~~
32 ~~multi-temporal inventories for 1990, 2000, and 2020 produced from 30 m resolution Landsat~~
33 ~~images.~~ The results show that, in 2020, 2234 lakes were derived from the Landsat images,
34 covering a total area of $86.31 \pm 14.98 \text{ km}^2$ with a minimum mapping unit of 5 pixels (4500
35 m^2), whereas, 7560 glacial lakes were derived from the Sentinel-2 images with a total area of
36 $103.70 \pm 8.45 \text{ km}^2$ with a minimum mapping unit of 5 pixels (500 m^2). ~~The results show that~~
37 ~~Landsat derived 2234 glacial lakes in 2020, covering a total area of $86.31 \pm 14.98 \text{ km}^2$ with a~~
38 ~~minimum mapping unit of 5 pixels (4500 m^2), whereas Sentinel derived 7560 glacial lakes in~~
39 ~~2020 with a total area of $103.70 \pm 8.45 \text{ km}^2$ with a minimum mapping unit of 5 pixels (500~~
40 ~~m^2).~~ The discrepancy shows that Sentinel-2 is able to detect a significant quantity of smaller
41 lakes than Landsat due to its finer spatial resolution. ~~The discrepancy implies that there is a~~
42 ~~significant quantity of small glacier lakes not recognized in existing glacial lake inventories~~
43 ~~and a more thorough inclusion of them require future efforts using higher resolution data.~~
44 Glacial lake data in 2020 was validated by Google Earth-derived lake boundaries with a
45 median (\pm standard deviation) differencediffering of $7.66 \pm 4.96 \%$ for Landsat-derived product
46 and $4.46 \pm 4.62 \%$ for Sentinel-derived product. The total number and area of glacial lakes
47 from consistent 30 m resolution Landsat images remain relatively stable despite a slight
48 increase from 1990 to 2020. A range of critical attributes have been generated in the dataset,
49 including lake types and mapping uncertainty estimated by an improved Hanshaw's equation.
50 This comprehensive glacial lake dataset has potential to be widely applied in studies on water
51 resource assessment, glacial lake-related hazards, glacier-lake interactions ~~and cryospheric~~
52 ~~hydrology,~~ and is freely available at <https://doi.org/10.12380/Glaci.msdc.000001> (Lesi et al.,
53 2022) ~~(Lesi et al., 2022)~~ ~~(Lesi et al., 2022)~~.

54 1 Introduction

55 Glaciers in High-mountain Asia (HMA) play a crucial role in regulating climate, supporting
56 ecosystems, modulating the release of freshwater into rivers, and sustaining municipal water
57 supplies (Wang et al., 2019; Viviroli et al., 2020) ~~(Wang et al., 2019; Viviroli et al., 2020)~~
58 ~~(Wang et al., 2019; Viviroli et al., 2020)~~, agricultural irrigation, and hydropower generation
59 (Pritchard, 2019; Nie et al., 2021) ~~(Pritchard, 2019; Nie et al., 2021)~~ ~~(Pritchard, 2019; Nie et~~
60 ~~al., 2021)~~. Most HMA glaciers are losing mass in the context of climate change (Brun et al.,
61 2017; Maurer et al., 2019; Shean et al., 2020; Bhattacharya et al., 2021) ~~(Brun et al., 2017;~~
62 ~~Shean et al., 2020; Bhattacharya et al., 2021; Maurer et al., 2019)~~ ~~(Brun et al., 2017; Maurer~~

63 et al., 2019; Shean et al., 2020; Bhattacharya et al., 2021), therefore, unsustainable glacier
64 melt is and the passing of peak water are reducing the hydrological role of glaciers (Huss and
65 Hock, 2018) (Huss and Hock, 2018) and impacting downstream ecosystem services,
66 agriculture, hydropower and other socioeconomic values (Carrivick and Tweed, 2016; Nie et
67 al., 2021) (Nie et al., 2021; Carrivick and Tweed, 2016) (Carrivick and Tweed, 2016; Nie et
68 al., 2021). The present and future glacier changes not only impact water supply for
69 downstream area but also alter the frequency and intensity of glacier-related hazards, such as
70 glacier lake outburst floods (GLOFs) (Nie et al., 2018; Rounce et al., 2020; Zheng et al.,
71 2021) (Nie et al., 2018; Zheng et al., 2021; Rounce et al., 2020) (Nie et al., 2018; Rounce et
72 al., 2020; Zheng et al., 2021), and rock and ice avalanches (Shugar et al., 2021) (Shugar et al.,
73 2021) (Shugar et al., 2021). Global glacial lake number and total area both increased between
74 1990 and 2018 in response to glacier retreat and climate change (Shugar et al., 2020) (Shugar
75 et al., 2020) (Shugar et al., 2020), which inevitably affected the risk of GLOFs, affecting the
76 allocation of freshwater resource. The Indus is globally the most important and vulnerable
77 water tower unit where glaciers, lakes and reservoir storage contribute about two-thirds of the
78 water supply (Immerzeel et al., 2020). Ice-marginal lakes store ~1% of total ice discharge in
79 Greenland and accelerate lake-terminating ice velocity by ~25% (Mankoff et al., 2020;
80 Carrivick et al., 2022). The An increasing frequency and risk of GLOFs (Nie et al., 2021;
81 Zheng et al., 2021) (Nie et al., 2021; Zheng et al., 2021) has been observed in the
82 Karakoram and Himalaya (Nie et al., 2021) (Nie et al., 2021) (Nie et al., 2021), and the
83 increasing risk of GLOFs (Zheng et al., 2021) (Zheng et al., 2021) (Zheng et al., 2021) is
84 threatening Asian existing and planned population and infrastructures existing and planned
85 infrastructures projects in the mountain ranges, such as the China-Pakistan Economic
86 Corridor (CPEC), as a flagship component of One Belt One Road Initiative (Battamo et al.,
87 2021; Li et al., 2021) where, (BRI) infrastructure construction projects, which aim to strength
88 connections between countries and promoting international trade and investment (Battamo
89 et al., 2021; Li et al., 2021). hydropower plants, railways, and highways. The northern section
90 of the CPEC passes through Pamir, Karakoram, Hindu Kush and Himalaya mountains where
91 droughts and glacier-related hazards are frequent and severe (Hewitt, 2014; Bhambri et al.,
92 2019; Pritchard, 2019), threatening local people, the existing, under-construction and planned
93 infrastructures, such as highways, hydropower plants and railways. Understanding the risk
94 posed by GLOFswater shortage and glacier-related hazards is a critical step to sustainable
95 development for the CPEC.

96 A large number of major infrastructure construction projects for the One Belt One Road
97 Initiative (BRI) play a fundamental role in strengthening the interconnection of infrastructure
98 between countries and promoting international trade and investment (Battamo et al., 2021; Li
99 et al., 2021) (Battamo et al., 2021; Li et al., 2021) (Battamo et al., 2021; Li et al., 2021).
100 Taking the Karakoram Highway for example, it is a unique land route to link China and
101 Pakistan. The China-Pakistan Economic Corridor (CPEC) is one of the BRI flagship
102 projects, as an example, the northern part of the China-Pakistan Economic Corridor where the
103 only roadhighway connecting China and Pakistan is located is a stronghold connecting many
104 countries. There are 6 hydropower stations with an installed capacity of more than 70MW in
105 this area, and 2 super-large hydropower stations with a total installed capacity of more than
106 8,800 are also under construction (as of 2021). These power stations are very important for

107 Pakistan, which has insufficient power resources. Many infrastructure projects such as
108 railways and pipelines may be planned in the future. However,
109 originating from Kashgar of the Xinjiang Uygur Autonomous region, China and
110 extending to Gwadar Port, Pakistan (Ullah et al., 2019; Yao et al., 2020) (Ullah et al., 2019;
111 Yao et al., 2020) (Ullah et al., 2019; Yao et al., 2020). The the northern section of the CPEC
112 passes through Pamir, Karakoram, Hindu Kush and Himalaya mountains where glacier
113 related hazards such as GLOFs are frequent and severe (Hewitt, 2014; Bhambri et al., 2019)
114 (Hewitt, 2014; Bhambri et al., 2019), threatening the existing, under construction and
115 planned infrastructures projects. Understanding the risk posed by GLOFs is a critical step to
116 disaster prevention for infrastructures across the CPEC (Figure 1). In the future, infrastructure
117 projects such as railways and pipelines may be planned.

118 Glacial lake inventories with a range of attributes benefit water resource assessment and
119 disaster risk assessment and disaster reduction related to glacial lake (Wang et al., 2020;
120 Carrivick et al., 2022) GLOFs, and contribute to predicting glacier-lake evolution and
121 cryosphere-hydrosphere interactions under climate change (Nie et al., 2017; Brun et al., 2019;
122 Maurer et al., 2019; Carrivick et al., 2020; Liu et al., 2020) (Nie et al., 2017; Brun et al.,
123 2019; Liu et al., 2020; Maurer et al., 2019; Carrivick et al., 2020) (Nie et al., 2017; Brun et
124 al., 2019; Maurer et al., 2019; Carrivick et al., 2020; Liu et al., 2020). Remote sensing is the
125 most viable way to map glacial lakes and detect their spatio-temporal changes in the high-
126 elevation zones where in situ accessibility is extremely low (Huggel et al., 2002; Quincey et
127 al., 2007) (Huggel et al., 2002; Quincey et al., 2007) (Huggel et al., 2002; Quincey et al.,
128 2007). Studies in glacial lake inventories using satellite observations have been heavily
129 conducted at regional scales recently, such as in the Tibetan Plateau (Zhang et al., 2015)
130 (Zhang et al., 2015) (Zhang et al., 2015), the Himalaya (Gardelle et al., 2011; Nie et al.,
131 2017) (Gardelle et al., 2011; Nie et al., 2017) (Gardelle et al., 2011; Nie et al., 2017), the
132 HMA (Wang et al., 2020; Chen et al., 2021) (Chen et al., 2021; Wang et al., 2020) (Wang et
133 al., 2020; Chen et al., 2021), the Tien Shan (Wang et al., 2013) (Wang et al., 2013) (Wang et
134 al., 2013), the Alaska (Rick et al., 2022) (Rick et al., 2022) (Rick et al., 2022), the Greenland
135 (How et al., 2021) (How et al., 2021) (How et al., 2021) and the northern Pakistan (Ashraf et
136 al., 2017) (Ashraf et al., 2017) (Ashraf et al., 2017). However, the latest glacial lake mapping
137 in 2020 is still absent along the CPEC. Among existing studies, Landsat archival images are
138 the most widely used due to their multi-decadal record of earth surface observations,
139 reasonably high spatial resolution (30 m), and publicly available distribution (Roy et al.,
140 2014) (Roy et al., 2014) (Roy et al., 2014). Freely available Sentinel-2 satellite images show
141 a better potential than Landsat in glacial lake mapping and inventories due to their higher
142 spatial resolution (10 m) and a global coverage, but have only been available since late 2015
143 (Williamson et al., 2018; Paul et al., 2020) (Williamson et al., 2018; Paul et al., 2020)
144 (Williamson et al., 2018; Paul et al., 2020). Glacial lake inventories using Sentinel-2
145 images are relatively scarce at regional scales, and studies of the latest glacial lake mapping as well
146 as comparisons of glacial lake datasets derived from Sentinel-2 and Landsat observations are
147 still lacking.

148 Discrepancies between various glacial lake inventories (Zhang et al., 2015; Shugar et al.,
149 2020; Wang et al., 2020; Chen et al., 2021; How et al., 2021) (Zhang et al., 2015; Shugar et
150 al., 2020; Wang et al., 2020; Chen et al., 2021; How et al., 2021) result from differences in

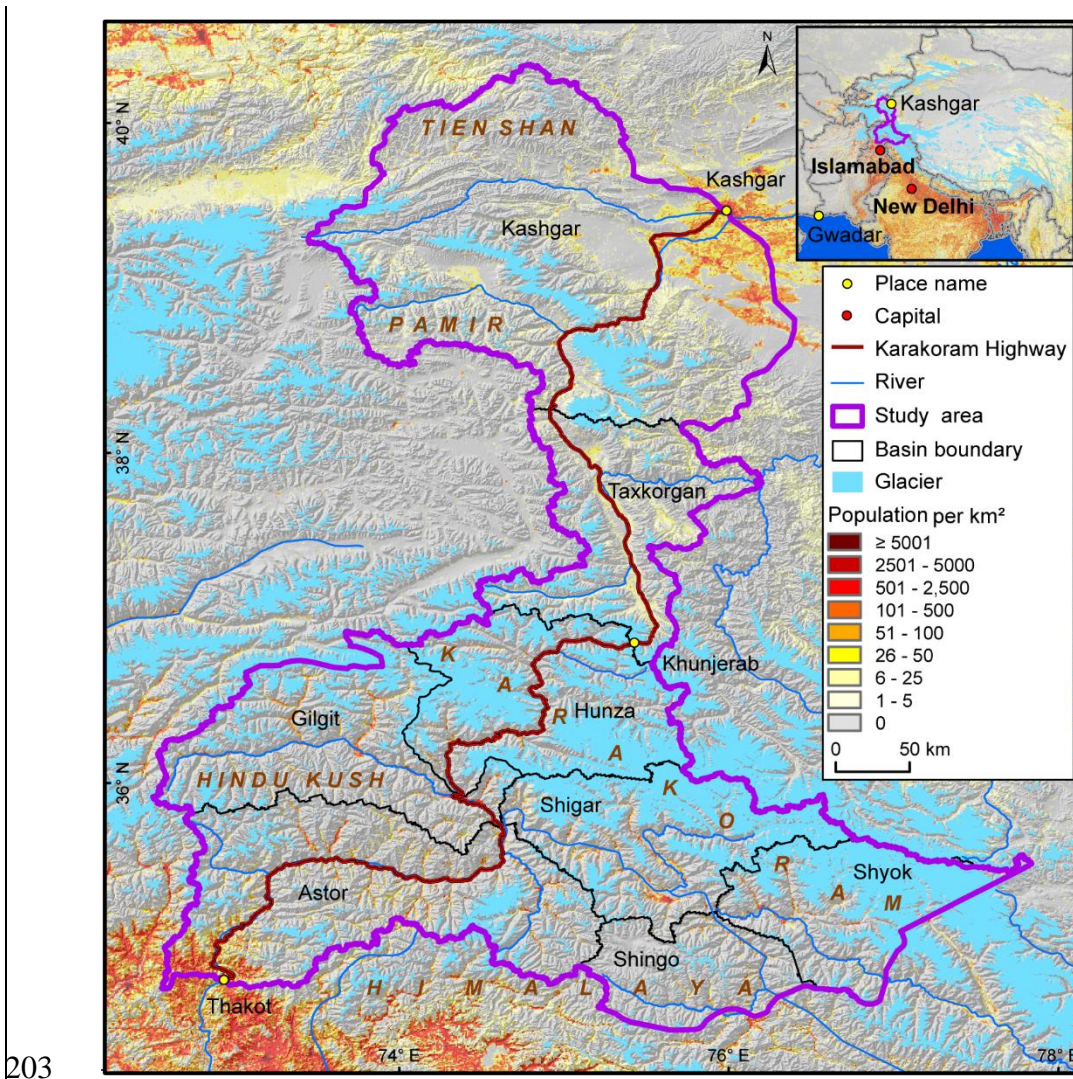
151 mapping methods, minimum mapping units, definition of glacial lakes, time periods, data
152 sources and other factors. For example, manual vectorization method was widely adopted at
153 the earlier stage for its high accuracy. However, it is time-consuming associated with high
154 labor intensity and is only practical at regional scales ([Zhang et al., 2015](#); [Wang et al., 2020](#))–
155 ([Zhang et al., 2015](#); [Wang et al., 2020](#)). Automated and semi-automated lake mapping
156 methods, such as multi-spectral index classification ([Gardelle et al., 2011](#); [Nie et al., 2017](#);
157 [Zhang et al., 2018](#); [How et al., 2021](#))–([Gardelle et al., 2011](#); [Nie et al., 2017](#); [Zhang et al.,](#)
158 [2018](#); [How et al., 2021](#)), have been developed to improve the efficiency of glacial lake
159 inventories using optical images, although manual modification is often unavoidable to assure
160 the quality of lake data impacted by cloud cover, mountain shadows, seasonal snow cover
161 and frozen lake surfaces ([Sheng et al., 2016](#); [Wang et al., 2017, 2018](#))–([Sheng et al., 2016](#);
162 [Wang et al., 2017, 2018](#)). Backscatter images from Synthetic Aperture Radar (SAR)
163 ([Wangchuk and Bolch, 2020](#); [How et al., 2021](#))–([Wangchuk and Bolch, 2020](#); [How et al.,](#)
164 [2021](#)) were used to remove the impact of cloud cover for lake mapping. Besides, other
165 approaches such as hydrological sink detection using DEM ([How et al., 2021](#))–([How et al.,](#)
166 [2021](#)) and land surface temperature-based detection method ([Zhao et al., 2020](#))–([Zhao et al.,](#)
167 [2020](#)) were also used for lake inventories. Different classification methods impact the results
168 of lake mapping and monitoring. [Dam type classification of glacial lakes provides a crucial](#)
169 [attribute for glacier lake interactions and risk assessment \(Emmer and Cuřín, 2021\)](#)–([Emmer](#)
170 [and Cuřín, 2021](#))–([Emmer and Cuřín, 2021](#)). So far, we are lacking a unified standard for the
171 classification system of glacial lakes ([Yao et al., 2018](#))–([Yao et al., 2018](#))–([Yao et al., 2018](#)).
172 Existing classification systems are [generally used mainly](#) for their [respective individual](#)
173 research purposes, mainly based on the relative positions of glacial lakes and glaciers, the
174 supply conditions of glaciers, and the attributes of dams. In addition to different classification
175 standards, the same type of glacial lakes may also have different names given by different
176 scholars. For example, ice-marginal ([Carrivick and Quincey, 2014](#); [Carrivick et al., 2020](#))–
177 ([Carrivick and Quincey, 2014](#); [Carrivick et al., 2020](#))–([Carrivick and Quincey, 2014](#);
178 [Carrivick et al., 2020](#)), ice-contact ([Carrivick and Tweed, 2013](#))–([Carrivick and Tweed, 2013](#))
179 ([Carrivick and Tweed, 2013](#)) and proglacial ([Nie et al., 2017](#))–([Nie et al., 2017](#))–([Nie et al.,](#)
180 [2017](#)) lakes all represent glacial lakes sharing the boundary with glaciers. Glacier lakes in
181 currently available datasets have been traditionally categorized by their spatial relationship
182 with upstream glaciers ([Gardelle et al., 2011](#); [Wang et al., 2020](#); [Chen et al., 2021](#))–([Gardelle](#)
183 [et al., 2011](#); [Chen et al., 2021](#); [Wang et al., 2020](#))–([Gardelle et al., 2011](#); [Wang et al., 2020](#);
184 [Chen et al., 2021](#)), and classification attributes considering the formation mechanism and the
185 properties of dams are rare or incomplete in the CPEC ([Yao et al., 2018](#); [Li et al., 2020](#))–([Yao](#)
186 [et al., 2018](#); [Li et al., 2020](#))–([Yao et al., 2018](#); [Li et al., 2020](#)). [Dam type classification of](#)
187 [glacial lakes provides a crucial attribute for glacier-lake interactions and risk assessment](#)
188 [\(Emmer and Cuřín, 2021\)](#). –Therefore, an up-to-date glacial lake dataset with critical,
189 quality-assured parameters (e.g. [lake area, volume and lake types](#)) is necessary.

191 This study aims to (1) [present an up-to-date glacial lake dataset in the CPEC in 2020 using](#)
192 [employ](#) both Landsat 8 and Sentinel-2 images [to create an up-to-date glacial lake dataset in](#)
193 [the CPEC](#) to accurately document its detailed lake distribution [in 2020](#); (2) [present two](#)
194 [historical glacial lake datasets for the CPEC to show extent in 1990 and 2000 reveal glacial](#)

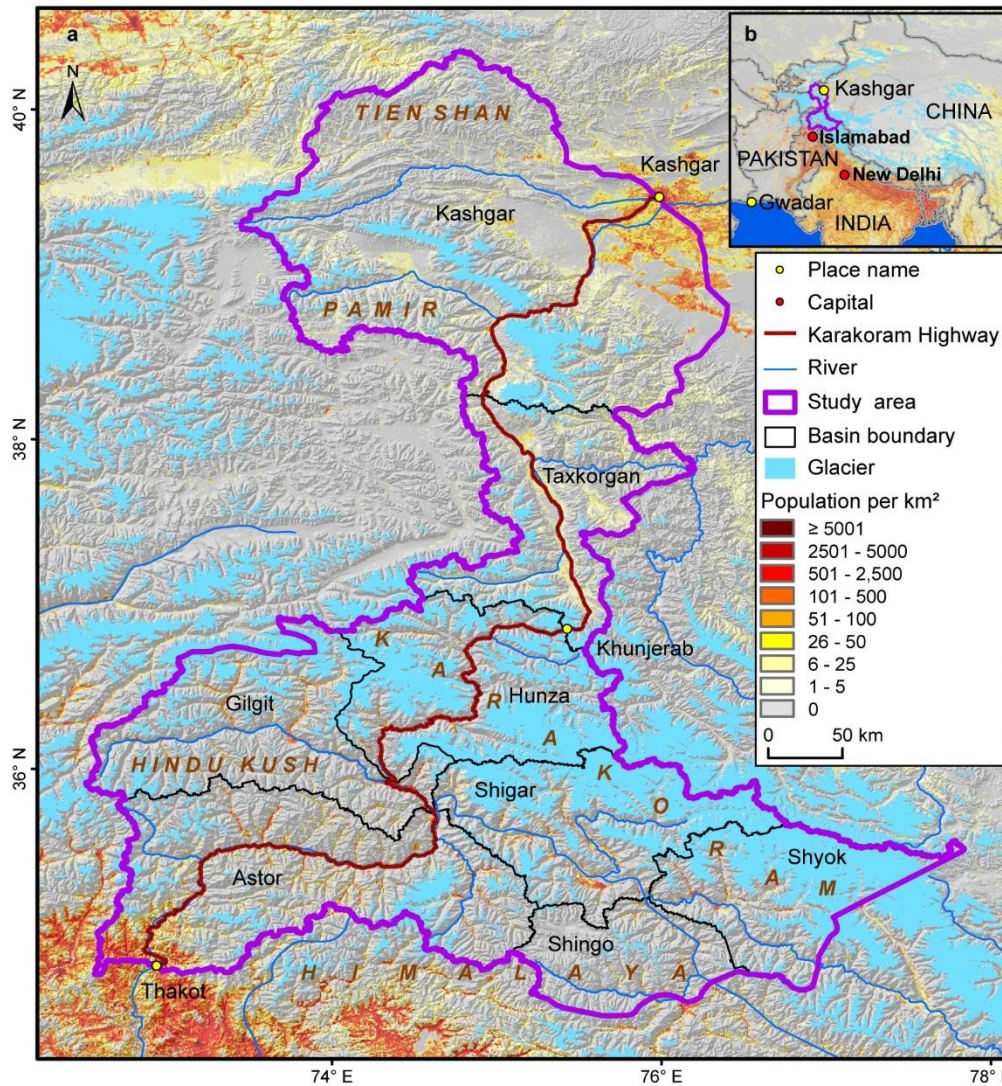
195 lake changes and the spatial heterogeneity across mountains and basins in the CPEC using
196 consistent 30-m Landsat images to reveal glacial lake changes at three time periods (1990,
197 2000 and 2020); and (3) generate share the glacial lake inventories with a range of critical
198 attributes for glacial lake inventories to benefit studies on water resource evaluation,
199 hazardous risk assessment of GLOFs, glacier changes and lake evolution glacio-hydrological
200 modeling in the HMA.

201

202 2 Study area



203



204

205 **Figure 14.** Location of the study area (ab) and associated with distribution of glaciers (RGI Consortium,
 206 2017) (RGI Consortium, 2017), mountains, basins and population (Rose et al., 2021) (a)-(a)., and its
 207 Location within of the CPCE (b).–

208

209 The northern part of the CPCE is selected as the study area (Figure 1). The CPCE, originating
 210 from Kashgar of the Xinjiang Uygur Autonomous region, China and extending to Gwadar Port,
 211 Pakistan (Ullah et al., 2019; Yao et al., 2020) (Ullah et al., 2019; Yao et al., 2020) (Ullah et al.,
 212 2019; Yao et al., 2020), :

213

is connecting China and Pakistan via the only Karakoram Highway.

214

215 The study area –(Figure 1)Figure 1 covers all the drainage basins along Karakoram Highway
 216 starting from Kashgar and ending at Thakot, with a total area of ~125,000 km². The upper Indus
 217 basins beyond the Pakistani-administrated border are excluded in this study due to little impact
 218 of GLOFs there on CPCE infrastructurespatial coverage of the CPCE. The entire study area
 219 is divided into eight sub-basins, covering most of the Karakoram with the highest altitude
 220 elevation up to 8611 m, western Himalaya and Tien Shan, eastern Hindu Kush and Pamir
 221 mountains. The 9710 glaciers in the study area cover a total area of 17,447 km² and nearly 60%
 of glaciers are distributed in the Karakoram (5818 glaciers with a total area of 14,067.52 km²)

(RGI Consortium, 2017) (RGI Consortium, 2017) (RGI Consortium, 2017). Most glaciers in the western Himalaya and eastern Hindu Kush are losing mass in the context of climate change (Kääb et al., 2012; Yao et al., 2012; Brun et al., 2017; Shean et al., 2020; Hugonnet et al., 2021) (Kääb et al., 2012; Yao et al., 2012; Shean et al., 2020; Brun et al., 2017; Hugonnet et al., 2021) (Kääb et al., 2012; Yao et al., 2012; Brun et al., 2017; Shean et al., 2020; Hugonnet et al., 2021), whereas the glaciers in the eastern Karakoram and Pamir have shown unusually little changes, including unchanged, retreated, advanced and surged glaciers (Hewitt, 2005; Kääb et al., 2012; Bolch et al., 2017; Brun et al., 2017; Shean et al., 2020; Nie et al., 2021) (Nie et al., 2021; Brun et al., 2017; Shean et al., 2020; Kääb et al., 2012; Hewitt, 2005; Bolch et al., 2017) (Hewitt, 2005; Kääb et al., 2012; Bolch et al., 2017; Brun et al., 2017; Shean et al., 2020; Nie et al., 2021). The spatially heterogeneous distribution and changes of glaciers are primarily explained as a result of differences in the dominant precipitation-bearing atmospheric circulation patterns that include the winter westerlies the Indian summer monsoon, their changing trends and their interactions with local extreme topography (Yao et al., 2012; Azam et al., 2021; Nie et al., 2021) (Azam et al., 2021; Nie et al., 2021; Yao et al., 2012) (Yao et al., 2012; Azam et al., 2021; Nie et al., 2021).

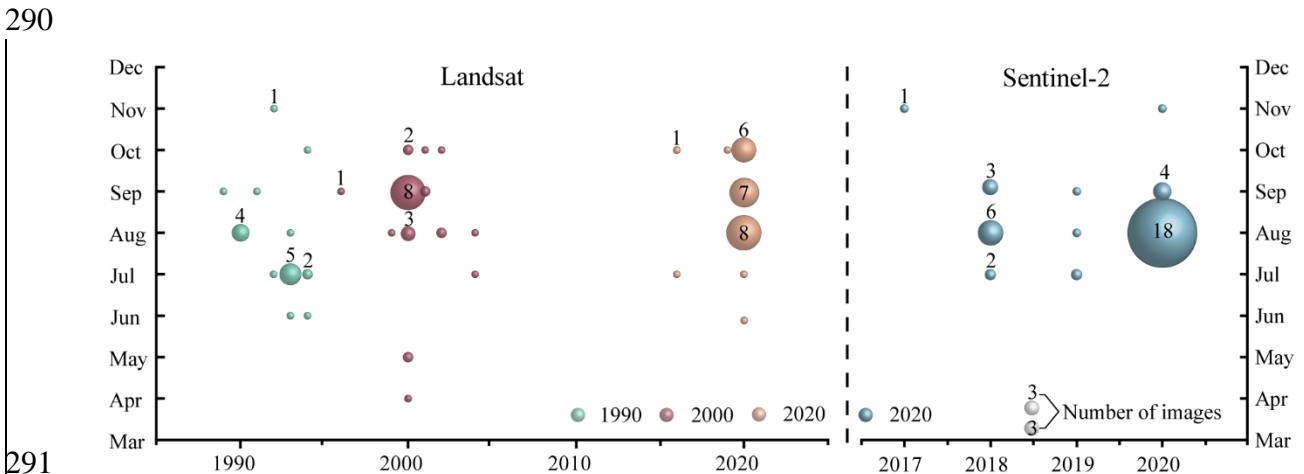
3 Data sources

Both Landsat and Sentinel-2 images have been employed to map glacial lakes between 1990 and 2020 in the CPEC (Figure 2 Figure 2). A total number of 71 Landsat Thematic Mapper (TM), Thematic Mapper Plus (ETM+) and Landsat 8 Operational Land Imager (OLI) images with a consistent spatial resolution of 30 m were downloaded from the United States Geological Survey Global Visualization Viewer (GloVis, <https://glovis.usgs.gov/>) to be used to create glacial lake inventories in 1990, 2000 and 2020. ~~4 scenes in 1990, 16 scenes in 2000 and 23 scenes in 2020 were used for each baseline year.~~ High-quality Landsat-5 images around 2010 are insufficient to cover the entire study area, so ~~we were unable to map lakes in 2010 due to Landsat-7's scan-line corrector errors and significant cloud covers~~ ~~we had to give up glacial lake mapping in 2010 as a result of Landsat 7's scan line corrector errors and significant cloud covers.~~ In addition, 39 Sentinel-2 images (23 scenes in 2020) were downloaded from Copernicus Open Access Hub (<https://scihub.copernicus.eu/>) to produce the 10-m resolution glacial lake inventory in 2020. All images used in this study have been orthorectified before download, but we still find that one Sentinel-2 image was not well matched with Landsat images, leading to the discrepancy between the two glacial lake datasets. We manually georeferenced the shifted image to minimize the difference between Sentinel and Landsat derived glacial lakes.

Cloud and snow covers heavily affect the usability of optical satellite images (Wulder et al., 2019) and their availability in the entire study area, so we took advantage of the images acquired before and after each of the baseline years 1990, 2000 and 2020 to construct the glacial lake inventories. Only 4 scenes-images in 1990 (the largest covering the study area), 16 images scenes in 2000 and 23 images scenes in 2020 were used for each-matching baseline year. Spatially, high-quality images in given baseline years were preferentially chosen, or we selected one or more alternative images acquired in adjacent years to delineate glacial lakes by removing the effect of cloud and snow covers. To minimize the impact of intra-annual changes of glacial lakes, most of used images (82% for Sentinel-2 and 75% for Landsat) were

265 acquired from August to October in the given baseline year with cloud coverage of <20% for
 266 each image. For some specific scenes where cloud cover exceeded the threshold of 20%, we
 267 selected more than one image to remedy the effect of cloud contamination (Nie et al., 2010,
 268 2017; Jiang et al., 2018) (Nie et al., 2010; Nie et al., 2017; Jiang et al., 2018) (Nie et al.,
 269 2010, 2017; Jiang et al., 2018).

270 Other datasets used include the Randolph Glacier Inventory version 6.0 (Pfeffer et al.,
 271 2014; RGI Consortium, 2017) (Pfeffer et al., 2014; RGI Consortium, 2017) (Pfeffer et al.,
 272 2014; RGI Consortium, 2017) and the Glacier Area Mapping for Discharge from the Asian
 273 Mountains (GAMDAM) glacier inventory (Sakai, 2019) (Sakai, 2019) (Sakai, 2019). These
 274 two glacier datasets were used to determine glacial lake types, such as ice-contact, ice-
 275 dammed and unconnected-glacier-fed lakes. The Shuttle Radar Topography Mission Digital
 276 Elevation Model (SRTM DEM) at a 1-arc second (30 m) resolution (Jarvis et al., 2008)–
 277 (Jarvis et al., 2008) (Jarvis et al., 2008) was employed to extract the altitudinal characteristics
 278 of the glacial lakes. The absolute vertical accuracy of the SRTM DEM is 16 m (90%) (Rabus
 279 et al., 2003; Farr et al., 2007) (Farr et al., 2007; Rabus et al., 2003) (Rabus et al., 2003; Farr et
 280 al., 2007). We also applied other published glacial lake datasets for comparative analysis.
 281 They include the glacial lake inventories of HMA in 1990 and 2018 downloaded from
 282 http://doi.org/10.12072/casnw.064.2019.db (Wang et al., 2020) (Wang et al., 2020) (Wang et
 283 al., 2020), the Third Pole region in 1990, 2000 and 2010 publicly shared at
 284 http://en.tpdatabase.cn/ (Zhang et al., 2015) (Zhang et al., 2015) (Zhang et al., 2015), the
 285 Tibet Plateau from 2008 to 2017 accessed at https://doi.org/10.5281/zenodo.3700282 (Chen
 286 et al., 2021) (Chen et al., 2021) (Chen et al., 2021), and the entire world in 1990, 2000 and
 287 2015 provided at https://nsidc.org/data/HMA_GLI/versions/1 (Shugar et al., 2020) (Shugar
 288 et al., 2020) (Shugar et al., 2020). In addition, field survey data collected between 2017 and
 289 2018 were also used to assist in lake mapping and glacial lake type classification.



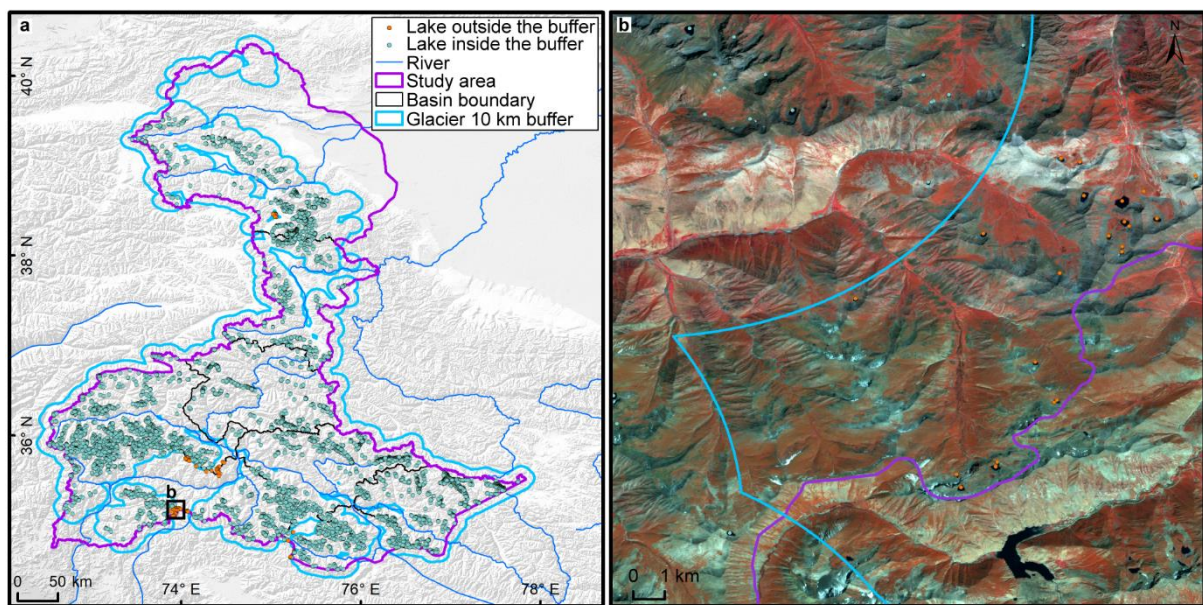
291
 292 **Figure 22.** Acquisition years and months of Landsat and Sentinel-2 images selected for glacial lake
 293 inventories. The bubble size indicates the available high-quality image number.

294 **4 Glacial lake inventory methods**

295 **4.1 Definition of glacial lakes**

296 We consider a glacial lake as one that formed as a result of modern or ancient glaciation.

297 Contemporary glacial lakes are easily recognized using a combination of glacier inventories
 298 and remote sensing images. Ancient glacial lakes can be identified from periglacial
 299 geomorphological characteristics, including moraine remnants and U-shaped valleys that are
 300 discernible from satellite observations (Post and Mayo, 1971; Westoby et al., 2014; Nie et al.,
 301 2018; Martín et al., 2021) (Post and Mayo, 1971; Nie et al., 2018; Martín et al., 2021;
 302 Westoby et al., 2014) (Post and Mayo, 1971; Westoby et al., 2014; Nie et al., 2018; Martín et
 303 al., 2021). A 10-km buffering distance of RGI 6.0 glacier boundaries that has been widely
 304 used in previous studies (Zhang et al., 2015; Wang et al., 2020), was created to help mapping
 305 glacial lakes. A few glacial lakes in the study area (a total of 84 lakes for Sentinel-2 dataset
 306 and 55 lakes for Landsat dataset in 2020) beyond the buffering zone, located near buffering
 307 boundaries, were intentionally included due to clear evidence of glaciation (Figure 3).
 308 Landslide-dammed lakes (Chen et al., 2017) (Chen et al., 2017) (Chen et al., 2017) in the
 309 periglacial environment buffering zone were excluded in our inventories because of their
 310 irrelevance to glaciation. We abandoned the definition that considers all lakes surrounding a
 311 specific buffering distance of other glaciers also as glacier lakes, although this definition has
 312 been widely used in previous studies assuming glacial meltwater as the main water supply
 313 (Zhang et al., 2015; Wang et al., 2020) (Zhang et al., 2015; Wang et al., 2020) (Zhang et al.,
 314 2015; Wang et al., 2020) (Zhang et al., 2015; Wang et al., 2020). This is because the
 315 contribution of glacial meltwater to the lake supply is arduous to be quantified without an
 316 accurate modeling of the cryosphere hydrological processes (Lutz et al., 2014) (Lutz et al.,
 317 2014) (Lutz et al., 2014) (Lutz et al., 2014). All glacial lakes in the study area were mapped
 318 according to our definition without regard to buffering distance of glaciers. We were able to
 319 implement this definition by carefully leveraging the spectral properties of glacial lakes and
 320 the periglacial geomorphological features that are often evident in remote sensing images (see
 321 more in sections 4.3 and 4.4).
 322



323
 324 **Figure 3.** The 10-km buffer zone of RGI 6.0 glacier boundaries (a) and Sentinel-derived glacial lakes
 325 located near buffering boundary within the study area (b).
 326

327 4.2 Interactive lake mapping

328 A human-interactive and semi-automated lake mapping method (Wang et al., 2014; Nie et al.,
329 2017, 2020)-(Wang et al., 2014; Nie et al., 2017; Nie et al., 2020)-(Wang et al., 2014; Nie et
330 al., 2017, 2020) was adopted to accurately extract glacial lake extents using Landsat and
331 Sentinel-2 images, based on the Normalized Difference Water Index (NDWI) (Mcfeeters,
332 1996)-(Mcfeeters, 1996)-(Mcfeeters, 1996). The NDWI uses the green and near infrared
333 bands and is calculated by the following equation:

$$334 \quad NDWI = \frac{Band_{Green} - Band_{NIR}}{Band_{Green} + Band_{NIR}} \quad (1)$$

335 where the green band and near infrared band were provided by both Landsat and Sentinel
336 multispectral images.

337 Specifically, the method calculated the NDWI histogram based on the pixels with each
338 user-defined and manually-drawn region of interest. The NDWI threshold that separates lake
339 surface from land was interactively determined by screening the NDWI histogram against the
340 lake region in the imagery (Wang et al., 2014; Nie et al., 2020)-(Nie et al., 2020; Wang et al.,
341 2014)-(Wang et al., 2014; Nie et al., 2020). This way, the determined NDWI threshold can be
342 well-tuned to adapt various spectral conditions of the studied glacier lakes. The raster lake
343 extents segmented by the thresholds were then automatically converted to vector polygons.
344 We first completed the glacial lake inventory in 2020 using this interactive mapping method,
345 and the 2020 inventory was then used as a reference to facilitate the lake mapping for other
346 periods.

347 The minimum mapping unit (MMU) was set to 5 pixels for both Landsat (0.0045 km²) and
348 Sentinel-2 images (0.0005 km²) in this study. MMU determines the total number and area of
349 glacial lakes in the dataset, and varies in the previous studies, such as 3 pixels (Zhang et al.,
350 2015)-(Zhang et al., 2015)-(Zhang et al., 2015), 6 pixels (Wang et al., 2020), or 9 pixels
351 (Chen et al., 2021)-(Chen et al., 2021)-(Chen et al., 2021) for a regional scale, or 55 pixels
352 (Shugar et al., 2020)-(Shugar et al., 2020)-(Shugar et al., 2020) for Landsat images for various
353 objectives and spatial a global scales. While a smaller threshold leads to a large quantity of
354 lakes mapped, it also generates larger mapping noises or uncertainties. Considering this
355 signal-noise balance and our focus on identifying prominent glacier lake dynamics in the
356 study area, we opted to use 5 pixels as the MMU for both Landsat and Sentinel-2 images.

357 Several procedures were taken to assure the quality assurance and quality control for lake
358 mapping, including 1) visual inspection and modification using the threshold-based mapping
359 method for each lake according to based on Landsat, Sentinel-2 and Google Earth high-
360 resolution images overlaying preliminarily lake boundary extraction at the given time period;
361 2) time series check for Landsat-derived glacial lake datasets from 1990 and 2020, and cross-
362 check between Landsat and Sentinel-2-derived lake dataset in 2020 to reduce errors of
363 omission and commission; 3) topological validation of glacial lake mapping, such as repeated
364 removal, elimination of small sliver polygons; and 4) logical check for lake types between
365 two classification systems of glacial lakes. False lake extents resulting from cloud or snow
366 cover, lake ice, and topographic shadows (Nie et al., 2017, 2020)-(Nie et al., 2020; Nie et al.,
367 2017)-(Nie et al., 2017, 2020) and were modified using previous semi-automated mapping
368 method based on alternative images acquired in adjacent years. Those procedures were time-

369 consuming, but helped to minimize the effect of cloud and snow covers, lake mapping errors,
370 and to maximize the quality of the produced lake product and the derived glacial lake
371 changes.

372 4.3 Classification of glacial lakes

373 Two glacial lake classification systems (GLCS) have been established based on relationship
374 of interaction between glacial lakes and glaciers as well as lake formation mechanism and
375 dam material properties. In the first GLCS (GLCS1), glacial lakes were classified into four
376 types based on their spatial relationship to upstream glaciers: supraglacial, ice-contact,
377 unconnected-glacier-fed lakes, and non-glacier-fed lakes according to Gardelle et al. ~~(2011)~~
378 ~~(2011)~~ and Carrivick et al. ~~(2013)~~ ~~(2013)~~ ~~(2013)~~. Alternatively, combining the
379 formation mechanism of glacial lakes and the properties of natural dam features, glacial lakes
380 were classified into five categories (herein named GLCS2) modified from Yao's classification
381 system ~~(2018)~~ ~~(2018)~~ ~~(2018)~~: supraglacial, end-moraine-dammed, lateral-moraine-dammed,
382 glacial-erosion lakes and ice-dammed lakes. Subglacial lakes were excluded due to the
383 mapping challenge from spectral satellite images alone. Characterization and examples for
384 each type are provided in ~~Table 1~~ ~~Table 1~~ and ~~Table 2~~ ~~Table 2~~. Individual glacial lakes were
385 categorized to the specific types for each GLCS according to available glacier inventory data,
386 geomorphological and spectral characteristics interpreted from Landsat, Sentinel and Google
387 Earth images. The synergy of these two GLCSs is beneficial to predicting glacier-lake
388 evolutions and providing fundamental data for water resource and glacial lake disaster risk
389 assessment. _

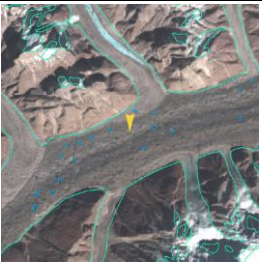


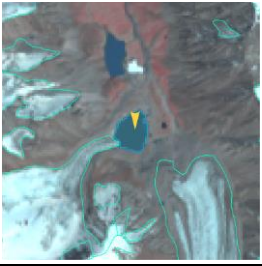
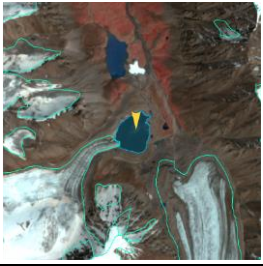
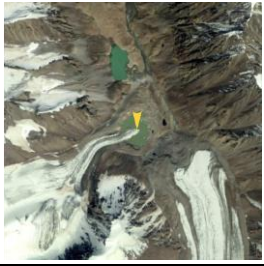
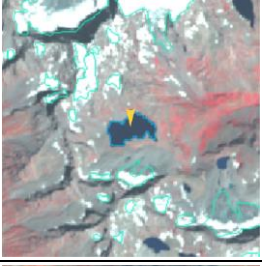
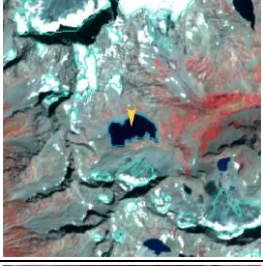
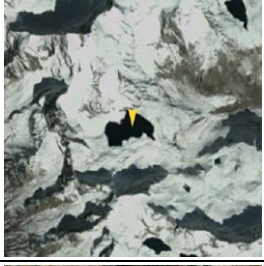
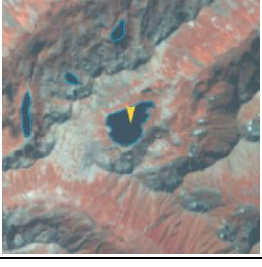
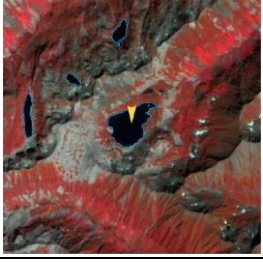

390

391

392

393 **Table 11.** Classification system of glacial lake types according to the relationship between glacial lakes
 394 and glaciers (© Google Earth 2019)._




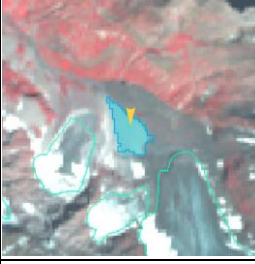
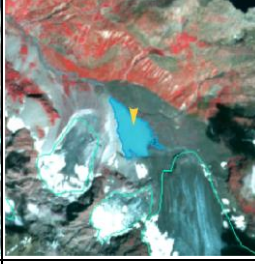


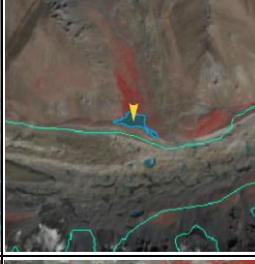





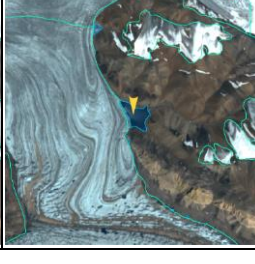
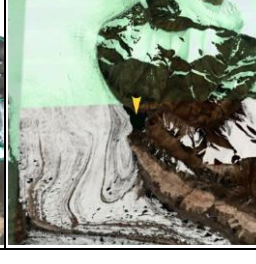
395 Glacier outlines are –from RGI 6.0 (RGI Consortium, 2017), and the yellow markers point to–
 396 therepresents easetarget glacial-lake.

Lake types	Characteristics	Landsat	Sentinel-2	Google Earth
Supraglacial	Lakes formed on the surface of glaciers, generally dammed by ice and thin debris. Case location: 35°43'49.74" N 76°13'53.88" E			
Ice-contact	Lakes dammed by moraine, ice or bedrock, supplied by glacial meltwater and shared boundary with glaciers. Case location: 39°09'32.40" N 73°43'12.00" E			
Unconnected-glacier-fed	Lakes currently supplied by upstream glacial meltwater but disconnected with glaciers. Case location: 35°47'60.00" N 72°55'15.60" E			
Non-glacier-fed	Lakes formed by glaciology, dammed by moraine or bed rock, and currently not supplied by glacial meltwater. Case location: 34°50'39.99" N 74°48'29.31" E			

397

398 **Table 22.** Classification system of glacial lake types according to the formation mechanism of glacial lakes
 399 and dam material properties (© Google Earth 2019)._

400 Glacier outlines from RGI 6.0 (RGI Consortium, 2017), and the yellow marker represents target lake. the
 401 yellow markers point to the case glacial lake.

Lake types	Characteristics	Landsat	Sentinel-2	Google Earth
Supraglacial	Lakes formed on the surface of glaciers, generally dammed by ice and thin debris. Case location: 36°46'7.39" N 74°20'7.59" E			
End-moraine-dammed	Lakes formed behind moraines as a result of glacier retreat and downwasting. Case location: 35°42'50.40" N 73°09'57.60" E			
Lateral-moraine-dammed	Lakes formed behind lateral glacial moraine ridges and dammed by debris, different from ice-dammed glacial lake. Case location: 38°28'45.62" N 75°20'52.30" E			
Glacial-erosion	Lakes formed in depressions created by glacial over-deepening. Bedrock dam dominates, partially superimposed by top moraine in rugged terrain. Dams are unclear in the satellite images. Case location: 35°55'55.56" N 73°38'20.13" E			
Ice-dammed	Lakes formed behind glaciers, dammed by glacier ices (partially covered by debris on the top). Case location: 35°28'31.32" N 77°30'46.81" E			

402

403 4.4 Attributes of glacial lake data

404 A total of 187 attribute fields were input into our glacial lake datasets (Table 3). They
 405 include lake location (longitude and latitude), lake elevation (centroid elevation), orbital
 406 number of the image source, image acquisition date, lake area, lake perimeter, lake types of the
 407 two GLCSs, mapping uncertainty, lake water volume and the country, sub-basin, and mountain

408 range associated with the lake. Amongst the attributes, lake location was calculated based on
 409 the centroid of each glacial lake polygon associated with the DEM, N represents northing and
 410 E represents easting. Orbital number of the image source was filled with the corresponding
 411 satellite image, with the codes expressed as “PxxxRxxx” or “Txxxxx”, where P and R indicate
 412 the path and row for Landsat image and T represents the tile of Sentinel-2 image associated
 413 with 5 digits code of military grid reference system. Area and perimeter were automatically
 414 calculated based on glacial lake extents. Lake water volume was estimated by area-volume
 415 empirical equation (Cook and Quincey, 2015). Lake types were attributed using the
 416 characterization and interpretation marks described in Section 4.3. Mapping uncertainty was
 417 estimated using our modified equation which will be introduced in section 4.5 and appendix
 418 tutorial. Located country, sub-basin and mountain range of each glacial lake was identified by
 419 overlapping the geographic boundaries of countries, basins and mountain ranges.

420
421

422 **Table 33.** ~~Classification system of glacial lake types according to the formation mechanism~~ Attributes ~~–of~~
 423 glacial lakes dataset and dam material properties.

Field Name	Type	Description	Note
FID or OBJECTID	Object ID	Unique code of glacial lake	Number
Shape	Geometry	Feature type of glacial lake	Polygon
Latitude	String	Latitude of the centroid of glacial lake polygon	Degree minute second
Longitude	String	Longitude of the centroid of glacial lake polygon	Degree minute second
Elevation	Double	Altitude <u>Elevation</u> of the centroid of glacial lake polygon	Unit: meter above sea level
IMGSOURCE	String	Path and row numbers for Landsat image based on World Reference System 2 or Tile number for Sentinel image based on military grid reference system	PxxxRxxx or Txxxxx
ACQDATE	String	Acquisition date of source image	YYYYMMDD
GLCS1	String	The first classification system of glacial lakes based on relationship of interaction between glacial lakes and glaciers	Supraglacial, Ice-contact, Unconnected-glacier-fed, None-glacier-fed

Field Name	Type	Description	Note
GLCS2	String	The second classification system of glacial lakes based on lake formation mechanism and dam material properties	Supraglacial, End-moraine-dammed, Lateral-moraine-dammed, Glacial-erosion and Ice-dammed
Basin	String	Basin name where glacial lake locates in	
Mountains	String	Mountain name where glacial lake locates in	
Country	String	Country name where glacial lake locates in	
Perimeter	Double	Perimeter of glacial lake boundary	Unit: meter
Area	Double	Area of glacial lake coverage	Unit: square meter
Uncertainty	Double	Uncertainty of glacial lake mapping estimated based on modified Hanshaw's equation (2014).--	Unit: square meter
<u>Volume</u>	<u>Double</u>	<u>Water volume of glacial lake estimated by area-volume empirical equation</u>	<u>Unit: square meter</u>
Operator	String	Operator of glacial lake dataset	Muchu, Lesi
Examiner	String	Examiner of glacial lake dataset	Yong, Nie

424

425 4.5 Error and uncertainty assessment~~Improved uncertainty estimating method~~

426 4.5.1 Improved uncertainty estimating method

427 We modified Hanshaw's ~~(2014)~~~~(2014)~~~~(2014)~~ equation that had been used to calculate lake-
428 area mapping uncertainty. Lake perimeter and displacement error are widely used to estimate
429 the uncertainty of glacier and lake mapping from satellite observation (Carrivick and
430 Quincey, 2014; Hanshaw and Bookhagen, 2014; Wang et al., 2020). Hanshaw and
431 Bookhagen ~~(2014)~~ proposed an equation to calculate the error of area measurement by the
432 number of edge pixels of the lake boundary multiplied by half of a single pixel area. The
433 number of edge pixels is simply calculated by the perimeter divided by the grid size. The
434 equation is expressed as below:

$$435 \text{Error}(1\sigma) = \frac{P}{G} \times 0.6872 \times \frac{G^2}{2} \quad \text{—————} \quad (2)$$

$$436 D = \frac{\text{Error}(1\sigma)}{A} \times 100\% \quad \text{—————} \quad \text{———} \quad (3)$$

437 Where G is the cell size of the remote sensing imagery (10 m for Sentinel-2 image and 30 m
 438 for Landsat image). P is the perimeter of individual glacial lake (m), and the ~~revised~~
 439 coefficient of 0.6872 (1σ), which means nearly 69% of the edge pixels are subject to errors
 440 (~~Hanshaw and Bookhagen, 2014~~), was chosen assuming
 441 that area measurement errors follow a Gaussian distribution. Relative error (D) was
 442 calculated by equation 3, in which A is the area of an individual glacial lake.

443 In the original equation 2, the number of edge pixels varies by the shape of lake and is
 444 indicated by $\frac{P}{G}$. However, the pixels in the corner are double counted (~~Figure 4~~
 445 ~~Figure 3~~). The total number of repeatedly calculated edge pixels equals the number of inner
 446 nodes. Therefore, we adjusted the calculation of the actual number of edge pixels as the
 447 maximum of edge pixels ($\frac{P}{G}$) subtracting the number of inner nodes. Accordingly, the equation
 448 of uncertainty estimation for lake mapping is modified as below:

$$449 \quad Error(1\sigma) = \left(\frac{P}{G} - N_{Inner}\right) \times 0.6872 \times \frac{G^2}{2} \quad (4)$$

450 Where N_{Inner} is the number of inner nodes (inflection points) of each lake. The modified
 451 equation is also suitable for lakes with islands (as illustrated in ~~Figure 4~~
 452 ~~Figure 3b~~).

452 For polygons without islands (~~Figure 4~~
 453 ~~Figure 3a~~), use the following equation:

$$453 \quad N_{Inner} = \left(\frac{N_{Total}-4-1}{2}\right) \quad (5)$$

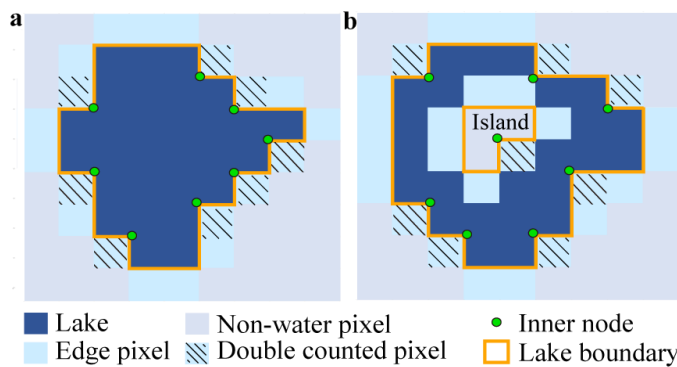
454 N_{Total} is the total number of nodes, including both the outer and inner. N_{Total} ~~were-is~~
 455 calculated by the “Field Calculator” in ArcGIS, in some cases, it is necessary to remove the
 456 redundant nodes before calculating the total number of nodes (See the ~~Supplement Appendix~~
 457 for more details). An inner node is a polygon vertex where the interior angle surrounding it is
 458 greater than 180 degrees. An outer node is the opposite of the inner node, where the interior
 459 angle is less than 180 degrees. We found that the outer nodes are usually four more than the
 460 inner nodes in our glacial lake dataset. The total nodes in ArcGIS contain one overlapping
 461 node to close the polygon, meaning the endpoint is also the startpoint. This extra count was
 462 deleted in the calculation (equation 5).

463 For polygons with island (~~Figure 4~~
 464 ~~Figure 3b~~) use the following equation:

$$464 \quad N_{Inner} = \left(\frac{N_{Total}-(N_{Island}+1)\times 5}{2}\right) \quad (6)$$

465 N_{Island} is the number of islands within each polygon. A calculation method of N_{Island} is
 466 given in the ~~Supplement Appendix~~.

467

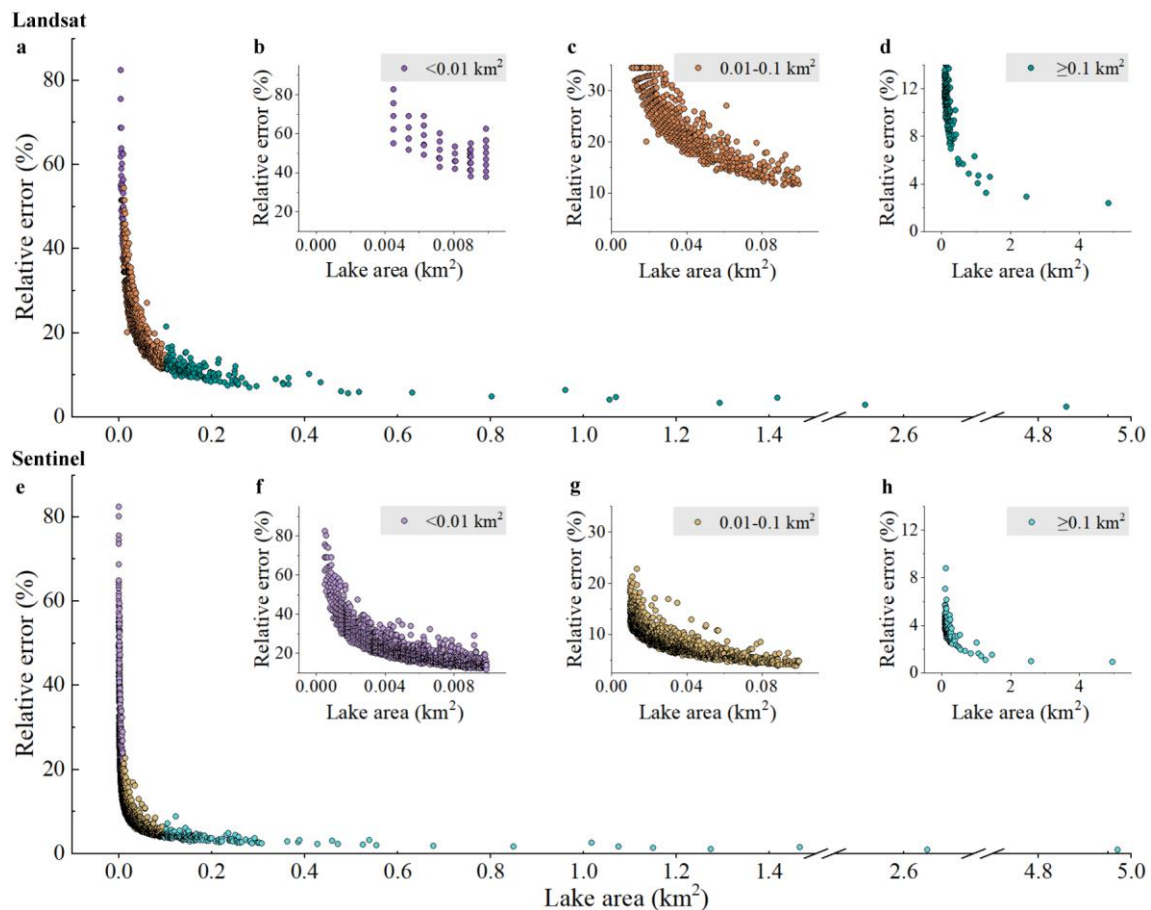


468
469 **Figure 43.** Sketch of estimating the actual edge pixels for uncertainty calculation of individual glacial lake
470 (with (a) and without islands (b)).
471

472 4.5.2 Validation of glacial lake mapping

473 A total of 89 glacial lakes were selected by stratified random sampling and manually digitized
474 based on the Google Earth high resolution images to further validate the absolute error of the
475 glacial lake mapping in 2020 due to lacking of field measurements for glacial lakes in the
476 study area. During the sampling, we set a regulation of minimum lake area greater than 4500
477 m² and relative differing between Landsat- and Sentinel-derived lake areas less than 18%
478 (nearly equaling to the average relative error of $\pm 17.36\%$ for Landsat lake mapping) to
479 minimize the effect of lake changes from multi-temporal satellite observations in circa 2020.
480 The 89 sample lakes range from 0.005 km² to 0.802 km² with a median (standard deviation)
481 size of 0.047 ± 0.134 km² and total area of 8.033 km² for Landsat-derived dataset, whereas
482 ranging from 0.005 km² to 0.849 km² with a median (standard deviation) size of 0.045 ± 0.144
483 km² and total area of 8.447 km² for Sentinel-derived dataset.

484 ~~The uncertainty estimated from our improved equation shows that the relative error of~~
485 ~~individual glacial lake decreases when lake size increases or cell size of remote sensing images~~
486 ~~reduces (Lyons et al., 2013; Carrivick and Quincey, 2014) (Lyons et al., 2013; Carrivick and~~
487 ~~Quincey, 2014) (Figure 4). Total area error of glacial lakes in study area is approximate ± 14.98~~
488 ~~km² and ± 8.45 km² in 2020 for Landsat and Sentinel images, respectively, and the average~~
489 ~~relative error is $\pm 17.36\%$ and $\pm 8.15\%$. Generally, small lakes have greater relative errors. For~~
490 ~~example, the mean relative error is 35.38% for Landsat derived glacial lakes between 0.0045~~
491 ~~and 0.1 km² and 10.63% for glacial lakes greater than 0.1 km². The mean area error of Sentinel-~~
492 ~~derived glacial lakes is almost one sixth of that extracted from Landsat images for glacial lakes~~
493 ~~of all or specific size group.~~



494
 495 **Figure 4.** Relationships between individual lake size and its estimated relative error for glacial lakes of all
 496 or specific size ranges in study area. Error estimation is based on the modified equation and lake data
 497 extracted from Landsat (a-d) and Sentinel images (e-h).
 498
 499

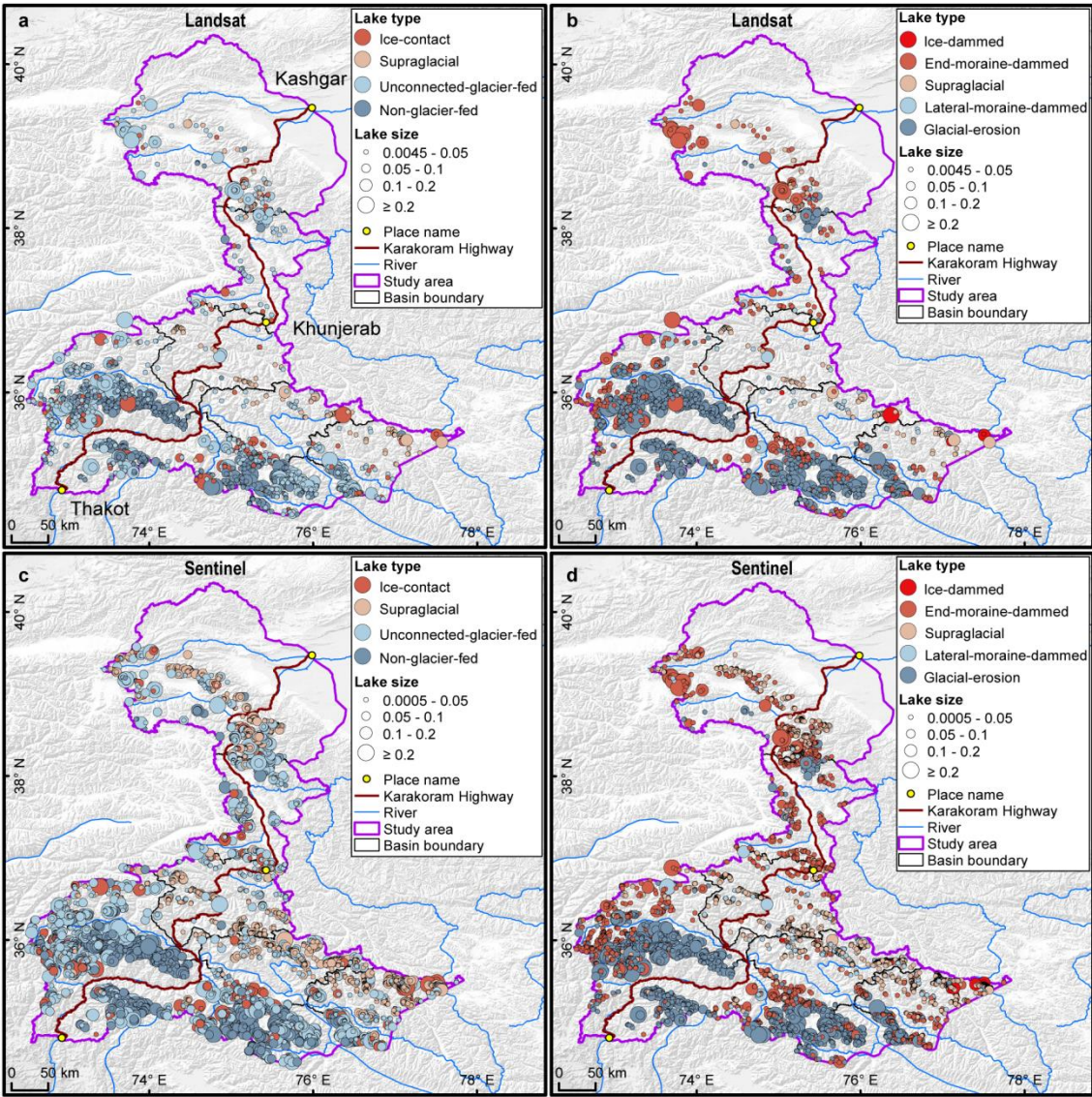
500 5 Results

501 5.1 Glacier lake distribution and changes observed from Landsat

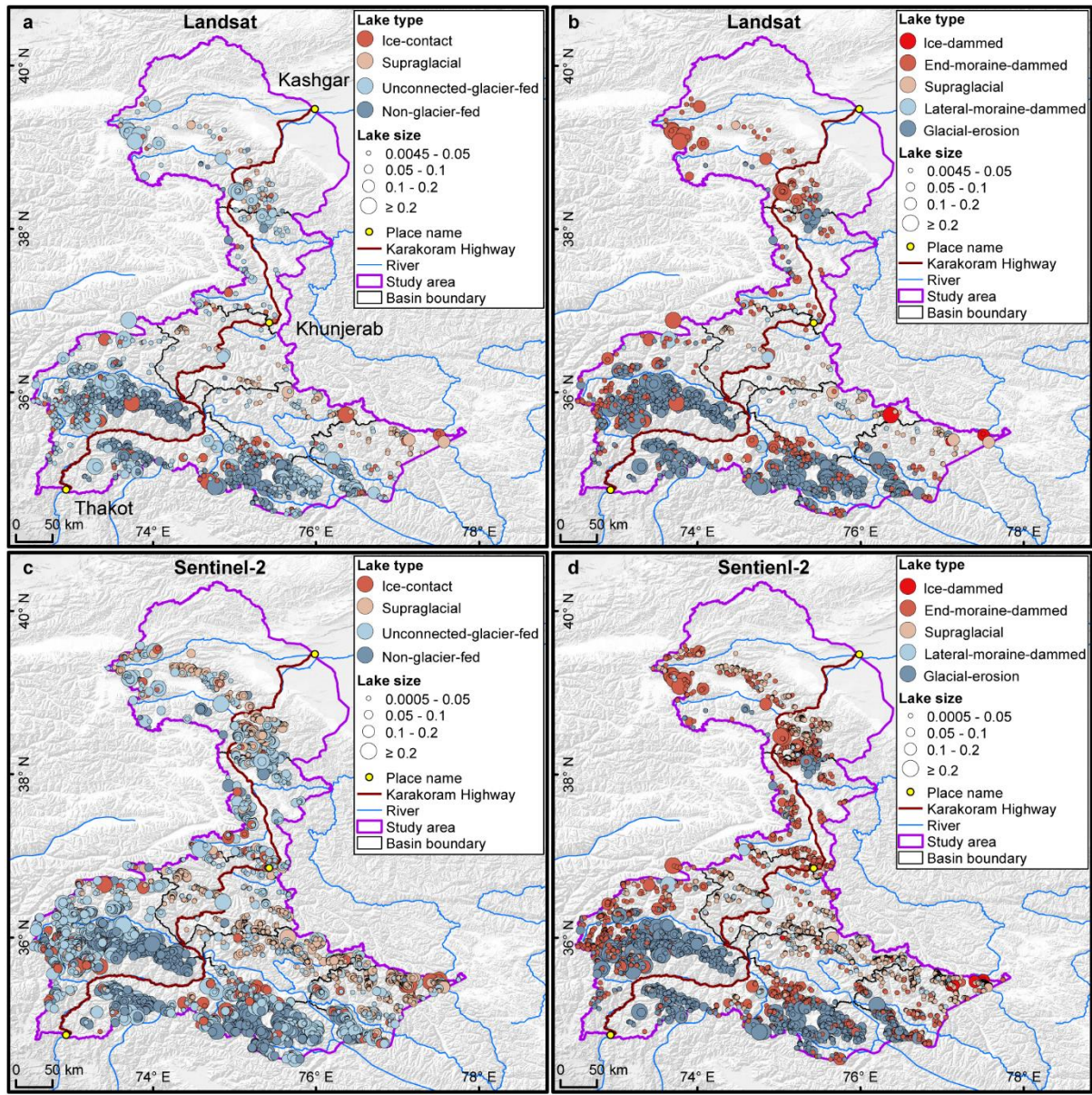
502 We mapped 2,234 glacial lakes for 2020 across the studied CPEC from Landsat-8 images,
 503 with a total area of $86.31 \pm 14.98 \text{ km}^2$ (Figure 5Figure 4Figure 5a and b). The majority of these
 504 glacial lakes (1,870 or 83.71%) are smaller than 0.05 km^2 and contribute 36.5% of the total
 505 area. 45 (2.01%) of the lakes are larger than 0.2 km^2 and contribute 28.8% of the total area
 506 (Figure 6). ~~With the increase of lake size, the abundance (count) of glacial lakes consistently~~
 507 ~~decreases but the total lake area first reduces and then increases.~~ Unconnected-glacier-fed
 508 lakes are dominant in the first classification system, followed by non-glacier-fed lakes
 509 (Figure 6Figure 5Figure 7) whereas glacial-erosion lakes dominate at both number (1478)
 510 and area (57.02 km^2) in the second classification system (Figure 7Figure 6Figure 8), followed
 511 by end-moraine-dammed lakes and supraglacial lakes. Among the classified lakes, 137 are
 512 ice-contact lakes and cover an area of 5.56 km^2 , implying a higher mean size of ice-contact
 513 lakes than supraglacial lakes.

514 ~~Glacial lakes are spatially heterogeneous among various mountain ranges and basins in the~~

515 study area. Himalaya sub-region has the maximum glacier lake count and area across the
 516 entire study area, followed by Hindu Kush. Supraglacial lakes are mainly distributed in the
 517 Karakoram but they cover less area than those in the Pamir. Tien Shan has fewer glacial
 518 lakes. Astor, Gilgit and Shingo basins have the largest percentages of glacier lakes in both
 519 number and area (>17%) (Figure 7Figure 9a), and each of the other basins contributes less
 520 than 10% except Kashgar basin in area due to several large ancient glacial lakes. Glacial
 521 lakes of less than 0.05 km² dominate in number within each basin and the total number
 522 decreases as lake size increases. Small lakes consistently account for the maximum
 523 percentage in area except Kashgar basin as a result of the disproportionately large lakes.
 524



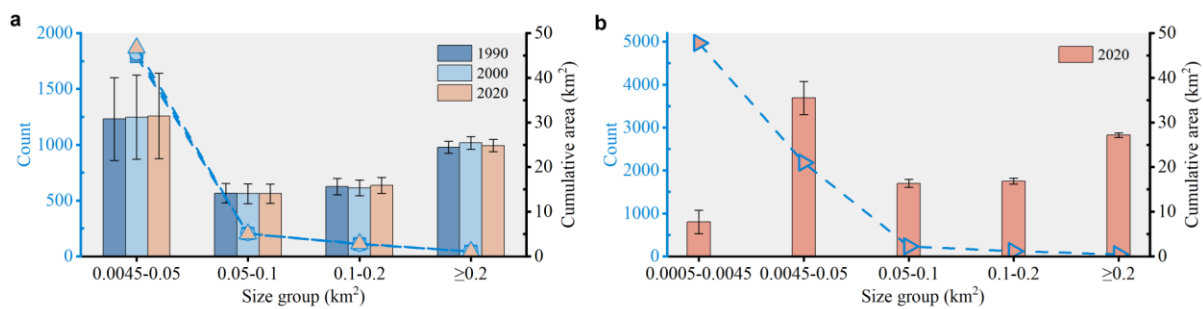
525



526

527 **Figure 545.** Distribution of glacial lakes in 2020 extracted from Landsat (a, b) and Sentinel-2 (c, d)
 528 images. Panels a and c are classified by GLCS1, and GLCS2 for sub-graph b and d.

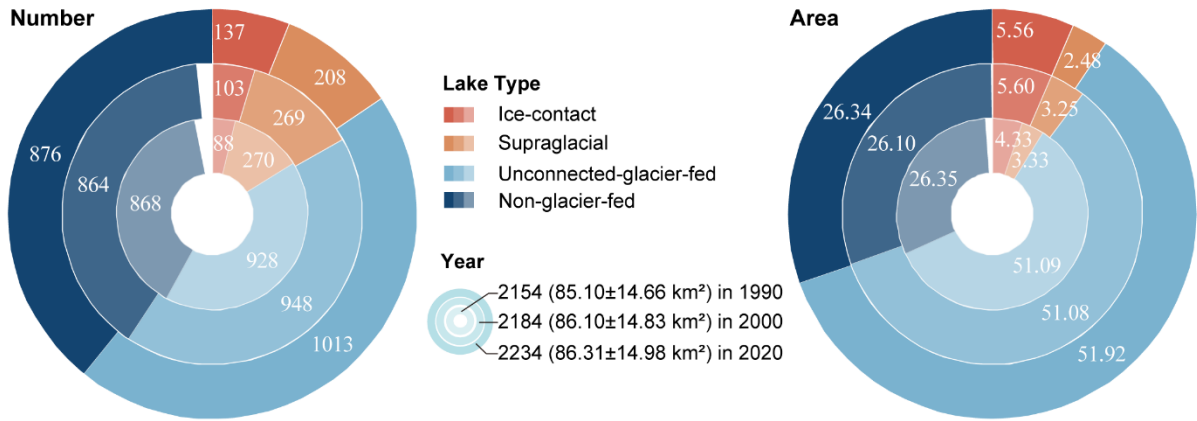
529



530

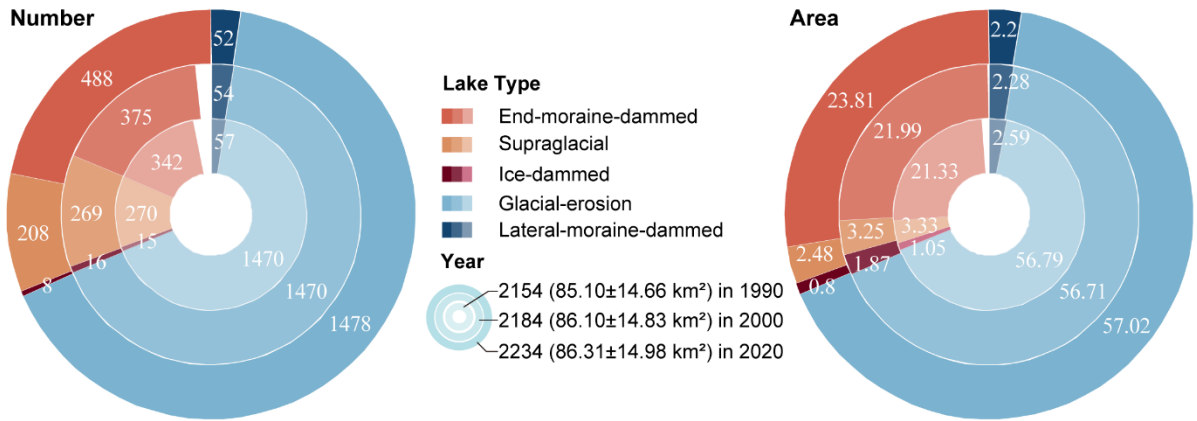
531 **Figure 6.** Statistics of different sizes of glacial lakes in the study area from 1990 to 2020. Panels a and b
 532 were derived from Landsat and Sentinel images, respectively.

533

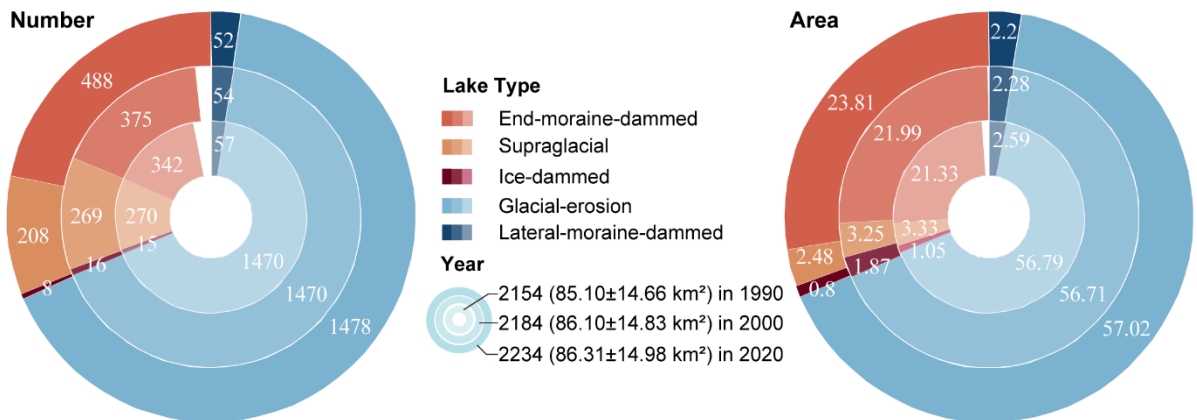


534

535 **Figure 657.** Number and area of different types of glacial lakes classified based on the condition of glacier
 536 supply in the study area (GLCS 1). The outermost ring represents glacial lake data in 2020, middle ring for
 537 2000 and innermost ring for 1990. Lake number and area in 2020 were selected as reference, meaning a
 538 concept of "100 %" for a complete ring. Labeled values are scaled in degrees rather the radius of rings.
 539

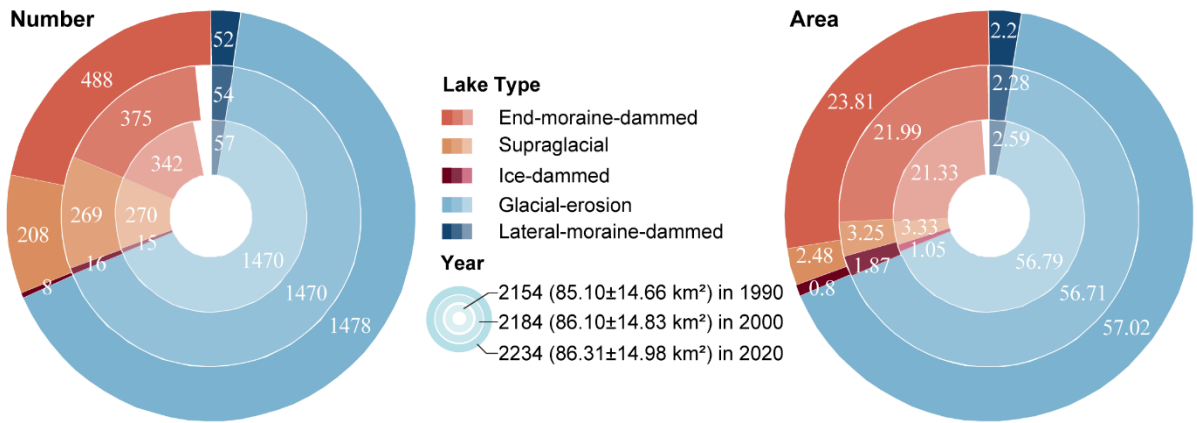


540



541

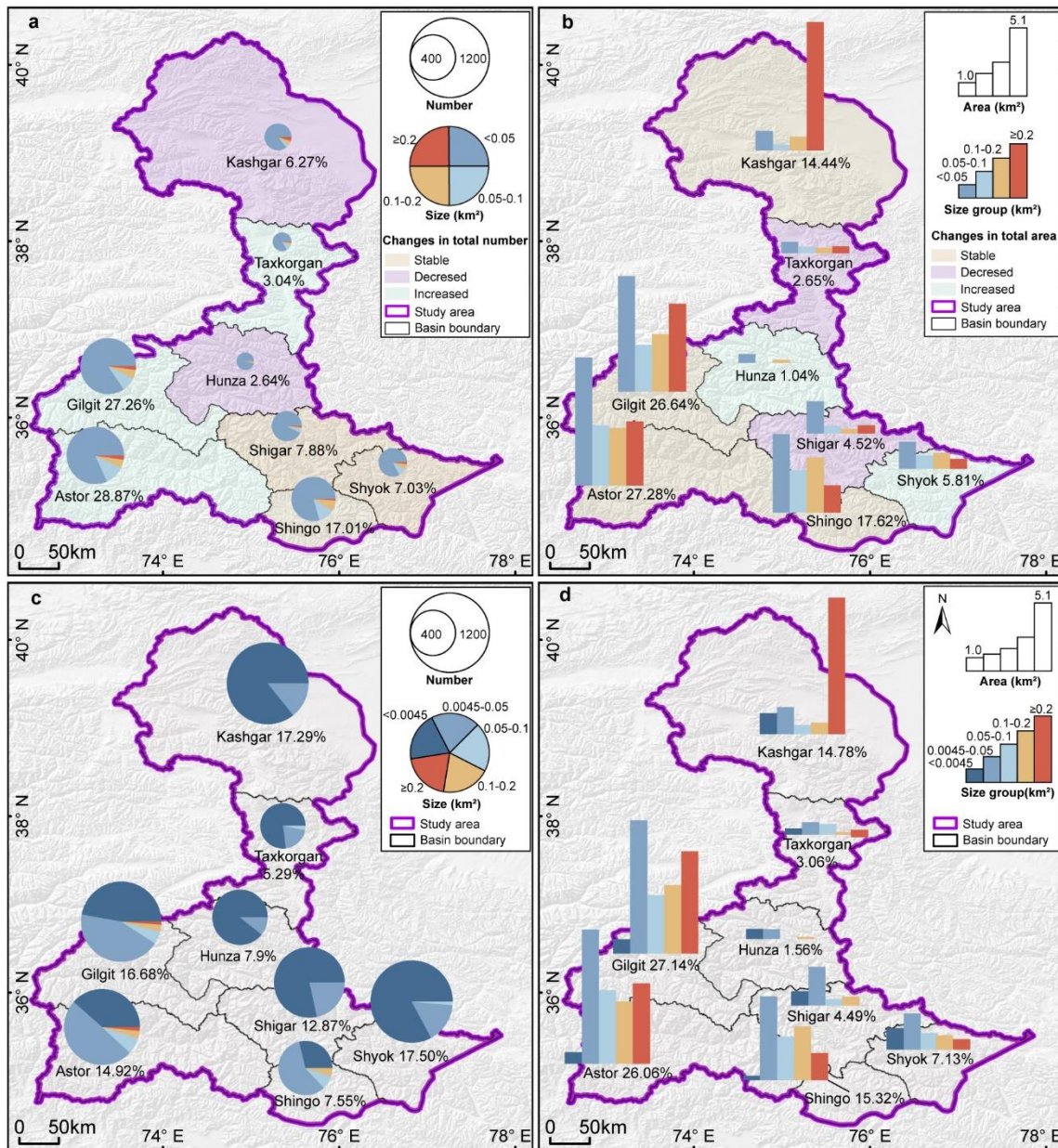
542 **Figure 768.** Number and area of different types of



543

544 glacial lakes classified based on glaciation and nature of dam in the study area (GLCS 2). The outermost
 545 ring represents glacial lake data in 2020, middle ring for 2000 and innermost ring for 1990. Lake number
 546 and area in 2020 were selected as reference, meaning a concept of "100 %" for a complete ring. Labeled
 547 values are scaled in degrees rather the radius of rings.

548



549 **Figure 79.** Distributions and changes in count and area of glacial lakes. Percent of glacial lakes in number
550 or area is labeled in each basin. Pie charts present the number of glacial lakes at various size groups –
551 between basins (a and c) and bar charts represent total area of glacial lakes at different size groups in each
552 basin (b and d). The background colors represent changes in total number and area between 1990 and 2020
553 based on Landsat derived dataset (a and b) and distribution of Sentinel-derived glacial lakes in 2020 among
554 basins are shown in sub-graphs c and d.
555

556
557 The total number and area of glacial lakes in the study remain relatively stable with a slight
558 increase between 1990 and 2020, and the changes in count and area among various types of
559 glacial lakes vary substantially (Figure 6Figure 5Figure 7 and Figure 7Figure 6Figure 8).
560 From 1990 to 2020, the total number of glacial lakes increased by 80 or 3.70%, while the area
561 grew by 1.21 km² (or 1.42%). Small lakes (<0.05 km²) continuously increased in number and
562 area, and contributed most in the total lake expansion (Figure 6). Lakes in the size group of
563 0.05–0.1 km² remained stable. The total area of lakes greater than 0.1 km² consistently –

increased.

In GLCS1, unconnected-glacier-fed lakes have the largest increase in number, followed by ice-contact and non-glacier-fed lakes, whereas supraglacial lakes decreased by 62 in count. Ice-contact lakes expanded by 1.24 km² (equaling an increase of 26% in ice-contact lakes), contributed one third of the total area increase. Supraglacial lakes decreased by 0.85 km² in area whereas the areas of unconnected-glacier-fed and non-glacier-fed lakes remained stable as a result of disconnections from glaciers (Figure 6Figure 5Figure 7).

In GLCS2, end-moraine-dammed lakes increased by 2.48 km² and contributed most of the glacier lake area expansion, whereas supraglacial, ice-dammed and lateral-moraine-dammed lakes decreased slightly in both number and area. Glacial-erosion lakes accounted for the maximum percentage (about 66% for both count and area) in each time period and remained stable (Figure 7Figure 6Figure 8).

Spatially, glacial lake changes in number and area vary among different mountain ranges and basins between 1990 and 2020 in the study area. Glacial lakes across the west Himalaya and Hindu Kush increased both in number and area between 1990 and 2020 whereas the total number of glacial lakes decreased in the Karakoram, Pamir and Tien Shan of study area (Table 4). The total area of glacial lakes continued to increase in the Hindu Kush, but decreased between 1990 and 2000 and increased between 2000 and 2020 in the Himalaya. The total number of glacial lakes continuously decreased in the Pamir and Tien Shan in the past three decades but increased at the first stage and decreased after in the Karakoram. The total area of glacial lakes persistently grew in the Pamir whereas fluctuated in the Tien Shan and Karakoram.

The majority of these glacial lakes (1,870 or 83.71%) are smaller than 0.05 km² and contribute 36.5% of the total area. 45 (2.01%) of the lakes are larger than 0.2 km² and contribute 28.8% of the total area. The total numbers of glacial lakes in Shingo, Shigar and Shyok basins were stable (Figure 7Figure 9a and b); however, the areal changes were less so, including a stable trend for Shingo, decreasing for Shigar, and increasing for Shyok. The total number of glacial lakes increased in the basins of Astor, Gilgit and Taxkorgan, whereas the total area of glacial lakes remained stable in Astor and Gilgit basins and decreased in Taxkorgan basin. The total numbers of lakes in Kashgar and Hunza basins decreased, whereas the total area of glacial lakes remained stable in Kashgar and increased in the Hunza basin.

Table 4. Distributions in count and area (km²) of glacial lakes among mountain ranges within the study area.

Source and year	Tien Shan	Karakoram	Pamir	Hindu Kush	Himalaya	Total
Landsat in 1990	10 (0.12)	370 (11.11)	178 (13.73)	780 (28.33)	816 (31.81)	2154 (85.10)
Landsat in 2000	7 (0.11)	393 (11.76)	163 (13.96)	792 (28.50)	829 (31.77)	2184 (86.10)
Landsat in 2020	5 (0.17)	334 (10.10)	182 (14.14)	835 (29.25)	878 (32.65)	2234 (86.31)
Sentinel in 2020*	11 (0.21)	479 (11.69)	262 (15.71)	880 (34.96)	959 (33.39)	2591 (95.96)

*Note: Glacial lake greater than 4500 m² are calculated for Sentinel 2 derived dataset in order to be in line with Landsat derived dataset.

601 5.2 Glacier lake distribution observed from Sentinel-2

602 Sentinel-derived results shows that there are 7,560 glacial lakes ($103.70 \pm 8.45 \text{ km}^2$) in 2020
 603 across the entire CPEC (~~Table 4~~~~Table 4~~~~Table 5~~) under a ~~minimum mapping unit~~MMU of 5
 604 pixels (500 m^2). ~~Compared with Landsat-derived product, glacial lakes from Sentinel-2 have~~
 605 ~~similar spatial distribution characteristics~~ ~~–(Figure 5~~~~Figure 7eb and d)~~~~among mountain~~
 606 ~~ranges, basins, types and altitudinal locations~~; meanwhile, a larger quantity of glacier lakes,
 607 ~~with more accurate boundaries and a greater total lake area, were generated from Sentinel-2~~
 608 ~~images. Similar to the pattern from Landsat mapping, the lake abundance extracted from~~
 609 ~~Sentinel images is inversely related to lake size (following a typical Pareto distribution).~~The
 610 smallest size class ($0.0005\text{-}0.0045 \text{ km}^2$) contains the maximum lake ~~count number~~ (4,969)
 611 but the least lake area ($7.73 \pm 2.62 \text{ km}^2$) (~~Table 4~~~~Table 4~~~~Table 5~~), which is not available in the
 612 Landsat-derived lake data due to a coarser spatial resolution. In each size class, there are also
 613 a higher number of larger glacial lakes from Sentinel than that from Landsat images. The
 614 discrepancy is mainly attributed to the inconsistency of spatial resolutions and image
 615 acquisition dates.

616
 617 **Table 445.** Count and area of glacial lakes mapped from Sentinel-2 and Landsat images in 2020 between
 618 various size classes.

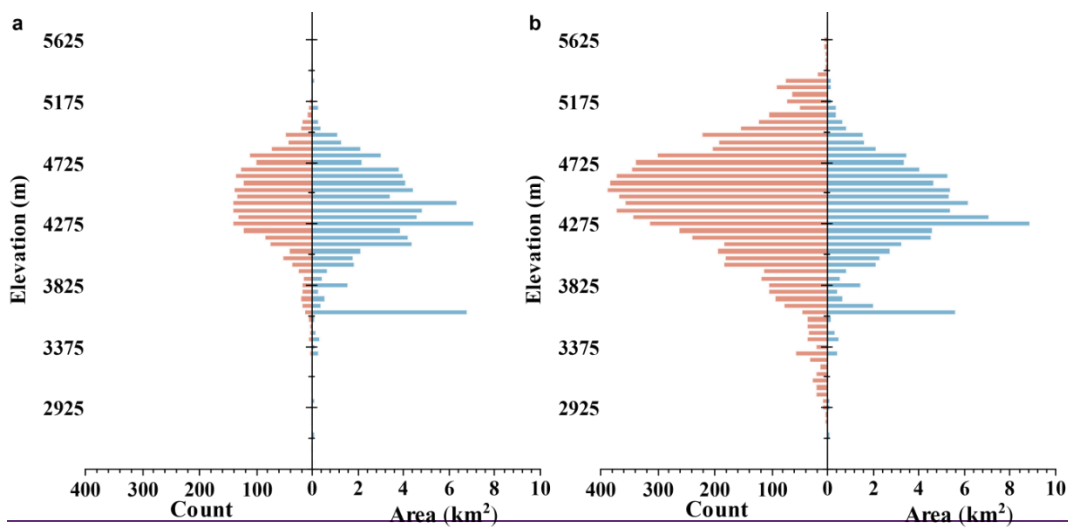
Lake size km ²	Glacial lakes from Sentinel-2 count (km ²)	Glacial lakes from Landsat count (km ²)	Overlap % (%)
0.0005-0.0045	4969 (7.73 ± 2.62)	—	—
0.0045-0.05	2182 (35.52 ± 3.72)	1870 (31.47 ± 9.57)	85.70 (88.60)
0.05-0.1	237 (16.37 ± 0.89)	204 (14.07 ± 2.18)	86.08 (85.95)
0.1-0.2	122 (16.88 ± 0.68)	115 (15.91 ± 1.83)	94.26 (94.25)
≥ 0.2	50 (27.20 ± 0.54)	45 (24.86 ± 1.40)	90.00 (91.40)
Total	7560 (103.70 ± 8.45)	2234 (86.31 ± 14.98)	—

619 Note:

620 Overlap % (%) represent the rates in count and area calculated by dividing Landsat-derived lake data by Sentinel-derived data
 621 in the same size class respectively.

622 ~~Compared with our Landsat-based product, glacial lakes from Sentinel-2~~
623 ~~have similar distribution characteristics (Figure 9c and d) among mountain~~
624 ~~ranges, basins, types and altitudinal locations (Figure 10); meanwhile, a larger~~
625 ~~quantity of glacier lakes, with more accurate boundaries and a greater total lake area,~~
626 ~~were generated from Sentinel-2 images. Taking altitudinal distribution for example, the number~~
627 ~~and size of glacial lakes in the study area appear follow a normal distribution against elevation for~~
628 ~~both Sentinel-2 and Landsat derived products (Figure 10). The elevation of all glacial lakes mapped~~
629 ~~in 2020 based on Sentinel-2 images ranged from 2500 m to 5750 m (a.s.l.), with 89.58% between 3600~~
630 ~~m and 5100 m and a mean altitude of 4421 m. The peak number appears between 4500 m and 4550 m~~
631 ~~whereas the maximum area emerges between 4250 m and 4300 m. The anomalously large area between~~
632 ~~3600 and 3650 m shows up in Fig. 10b because of several large lakes. Although Landsat derived~~
633 ~~lakes show a similar distribution pattern to Sentinel derived lakes, the lake count and~~
634 ~~area in each altitudinal band are greater in the Sentinel product due to the improved~~
635 ~~spatial resolution and image quality.~~

636



637

638 ~~Figure 10. Altitudinal distribution of glacial lakes in 2020 derived from~~
639 ~~Landsat (a) and Sentinel images (b)~~

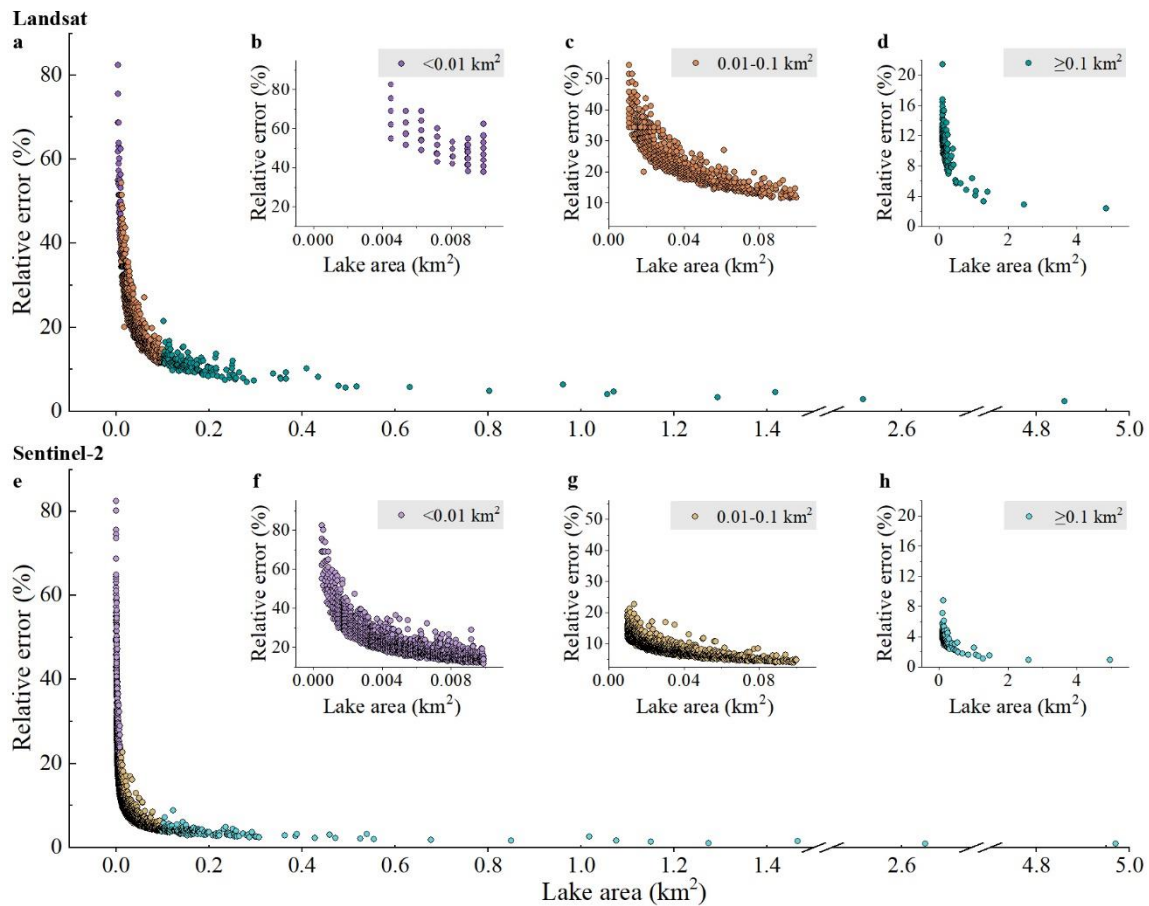
640

641 **6 Discussions**

642 6.1 Error and uncertainty of lake mapping

643 The uncertainty estimated from our improved equation shows that the relative error of
644 individual glacial lake decreases when lake size increases or cell size of remote sensing
645 images reduces (Lyons et al., 2013; Carrivick and Quincey, 2014) (Figure 8). Total area error
646 of glacial lakes in study area is approximate $\pm 14.98 \text{ km}^2$ and $\pm 8.45 \text{ km}^2$ in 2020 for Landsat
647 and Sentinel-2 dataset, respectively, and the average relative error is $\pm 17.36\%$ and $\pm 8.15\%$.
648 Generally, small lakes have greater relative errors. For example, the mean relative error is
649 35.38% for Landsat derived glacial lakes between 0.0045 and 0.1 km^2 and 10.63% for glacial
650 lakes greater than 0.1 km^2 . The mean area error of Sentinel-derived glacial lakes is almost
651 one sixth-third of that extracted from Landsat images for glacial lakes of all or specific size
652 group. Because the relative error was estimated as a function of satellite image spatial
653 resolution and lake perimeter, the calculated error for large lake is proportionally smaller than
654 that of small lake (Salerno et al., 2012) and the error for Landsat-derived lake is naturally
655 greater than that of Sentinel-derived lake at the same size group.

656



657

658

659

660

661

662

663

664

665

666

667

668

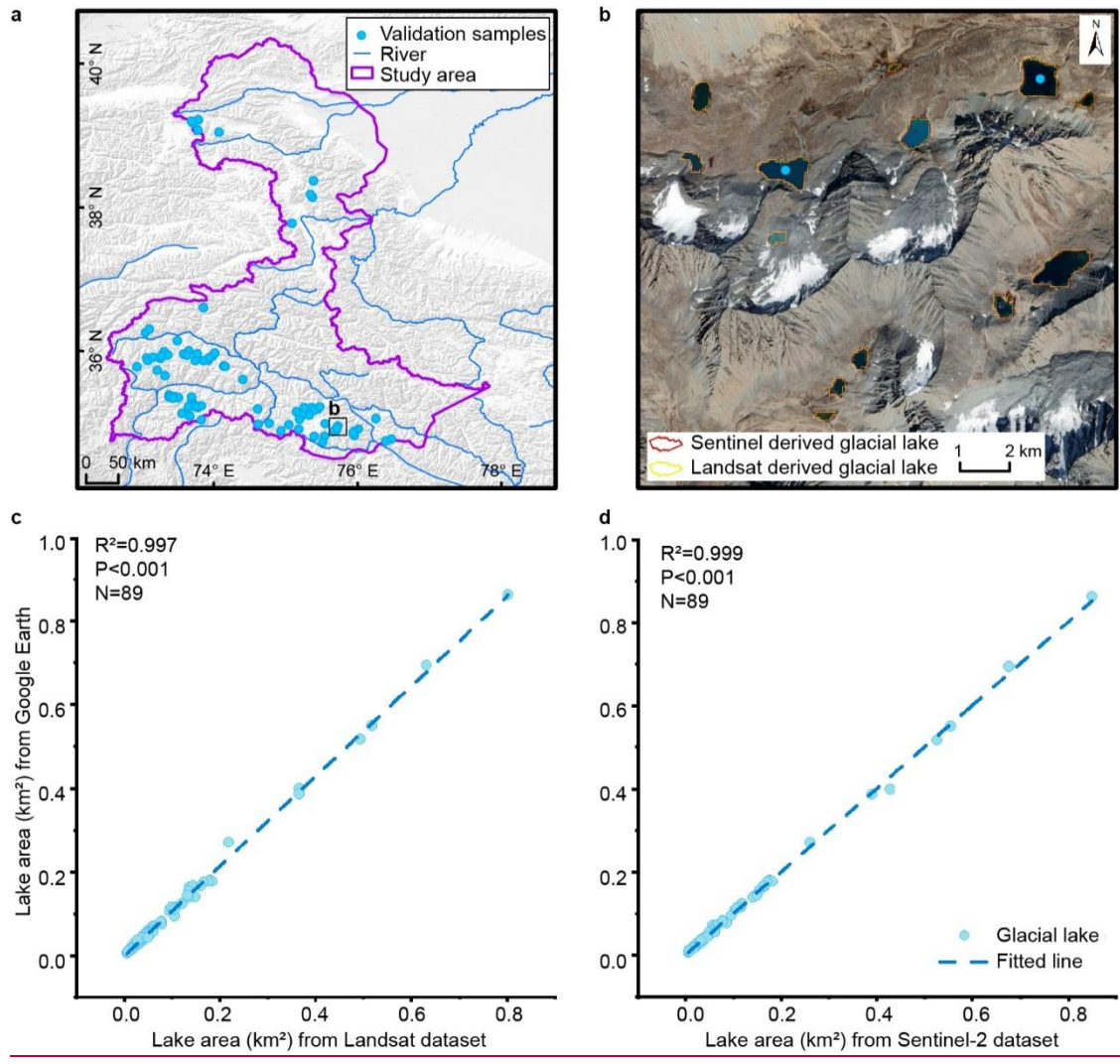
669

670

671

Figure 8. Estimated relative error for glacial lakes of all or specific size ranges in study area. Error estimation is based on the modified equation and lake data extracted from Landsat (a-d) and Sentinel-2 images (e-h).

Our Landsat- and Sentinel-derived glacial lake dataset well-match well lake boundaries in Google Earth high resolution images (Figure 9). A dense cluster of validation samples along the 1:1 line indicates a high accuracy in lake mapping (Figure 9c and d). The error of 89 sample lakes is 5.48% in total area between Landsat- and Google Earth-derived data, whereas 0.61% for Sentinel- and Google Earth-derived data. The median (\pm standard deviation) in discrepancy of individual lake area is 7.66 ± 4.96 % for Landsat- and Google Earth-derived data, whereas 4.46 ± 4.62 % for Sentinel- and Google Earth-derived data. Our glacial lake dataset shows a satisfactory mapping accuracy, and of which Sentinel-derived lake data performs more accurate than those from Landsat images.

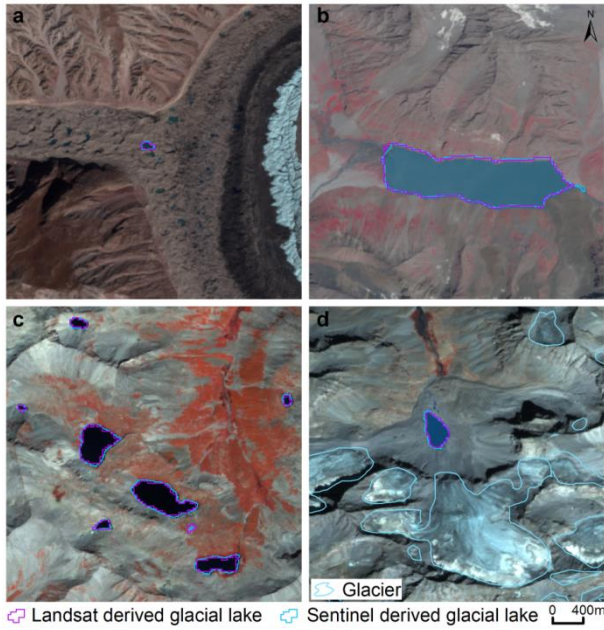


672

673 **Figure 9.** Distribution of validation samples (a), comparison of glacial lakes derived from Landsat and
 674 Sentinel-2 overlaying Google Earth image (© Google Earth 2019) in a zoomed site (b), and glacial lake
 675 product validated by Google Earth derived lake boundaries (c and d).

676 **6.12** Comparison of Sentinel-2 and Landsat derived products

677 Glacial lakes from Landsat and Sentinel-2 images have a high consistency in number and
 678 area with overlap rates from approximately 865.7% to 94.26% for all lakes greater than
 679 0.0045 km² approximately (Table 4Table 4Table 5), implyindicating a good potential for
 680 coordinated utility with Landsat archived observation (Figure 10Figure A8Figure 11). Lake
 681 extents extracted from Landsat and Sentinel images match well for various types and sizes
 682 (Figure 10 and Table 4Table 4). The best consistency rate reaches 94% for the glacial lakes
 683 between 0.1 km² and 0.2 km². The difference in area of glacial lakes extracted from Landsat
 684 and Sentinel-2 images generally lies within the uncertainty ranges.



685

686

687

688

689

690

691

692

693

694

695

696

697

698

699

700

701

702

703

704

705

706

707

708

709

710

711

712

713

Figure 10. High consistency of lake extents extracted from Landsat and Sentinel-2 images. Lake types shown include supraglacial (a), glacier-fed moraine-dammed (b), unconnected glacial-erosion lake without glacier melt supply (c) and glacier-fed moraine-dammed lakes (d).

The high consistency of Sentinel-2 and Landsat-derived glacial lake products in 2020 assures the value of our lake dataset. Taking the usage in assessing GLOFs as an example, we set 0.05 km^2 as the area threshold to select object lakes, including ice-contact lakes and ice-dammed lakes that are the most active lakes and source lakes of GLOFs in the CPEC (Nie et al., 2021). A total of 24 and 29 ice-contact lakes were selected from Landsat and Sentinel-derived products, respectively. Among them, there were 4 ice-dammed lakes from the Landsat-derived product and 5 from the Sentinel-derived product. These selected lakes can be used for GLOFs hazard evaluation. Because of the high consistency between our Landsat and Sentinel-based mappings, users may have the flexibility to customize the lake size criteria to facilitate their specific purposes.

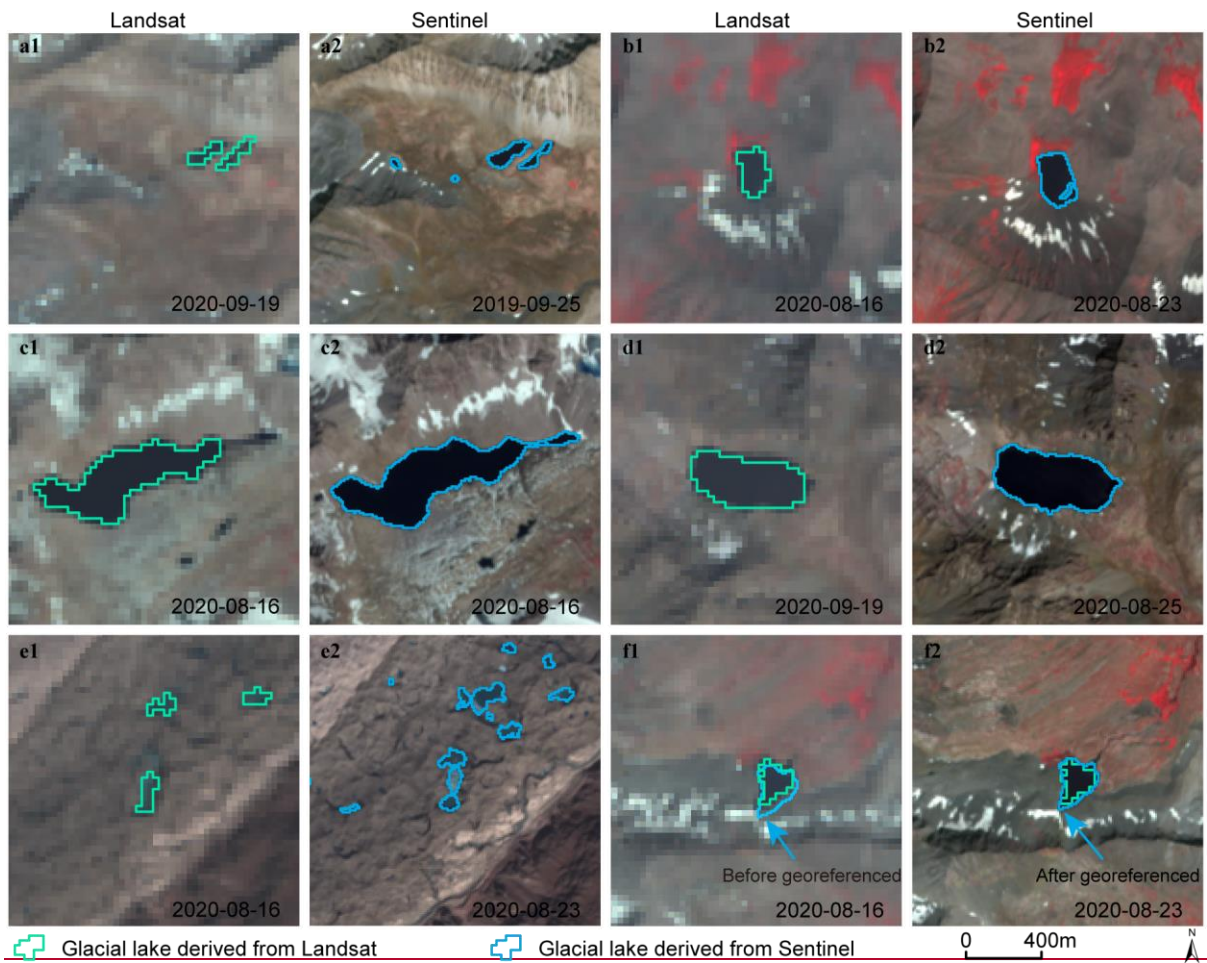
Spatial resolution of satellite images plays a primary role in the discrepancies in count and area of glacial lakes extracted from Landsat (30 m) and Sentinel-2 (10 m) observations. Due to a finer spatial resolution, Sentinel-2 images can extract more glacial lakes and more accurate extents than those from Landsat images. We set the same 5 pixels as the **minimum-mapping unit (MMU)** for both Landsat and Sentinel-2 images, which corresponds to a minimum area of 0.0045 km^2 and 0.0005 km^2 , respectively. The minimum mapping area results in generating nearly 5000 more lakes from Sentinel-2 images than from Landsat images, causing the greatest discrepancy in number of the two glacial lake products (Table 4 Table 5), such as Figure 11 Figure 8 Figure 12a. Small lakes such as supraglacial lakes play an important role in understanding analyzing glacier evolution meltwater runoff and supraglacial drainage systems (Liu and Mayer, 2015; Miles et al., 2018) (Miles et al., 2018; Liu and Mayer, 2015) (Liu and Mayer, 2015; Miles et al., 2018), implying a potential of Our dataset has huge application prospects in can be used not only for GLOFs evaluation,

714 ~~but also for to be applied in~~glacial lake evolution simulation and glacio-hydrological
715 ~~prediction~~studies of glacier-lake evolutions. Meanwhile, Sentinel-2 images are able to depict
716 boundaries of glacial lake with a lower uncertainty, (Figure 12b-d). For example, as for some
717 small islands and narrow channels (Figure 11Figure 8Figure 12b and c) were mapped from
718 Sentinel-2 imagery that were unable to be detected in Landsat imagery.

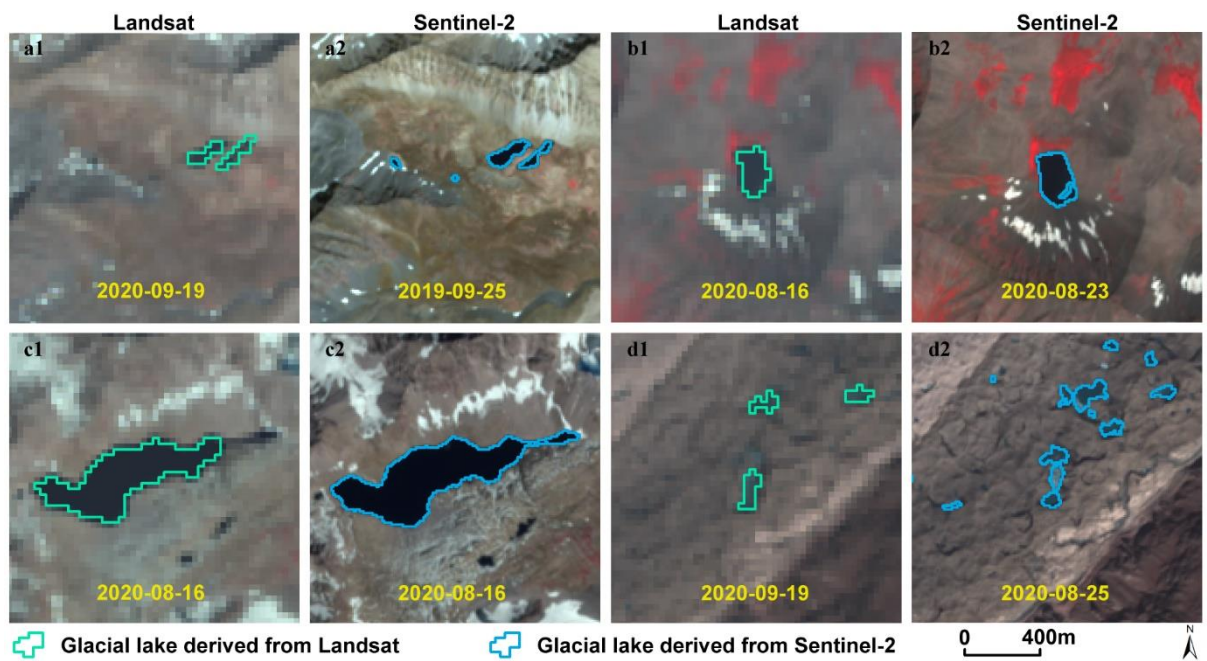
719 Different acquisition dates between Sentinel-2 and Landsat images also contribute to the
720 discrepancy of those two glacial lake datasets. Acquiring same-day images from the two
721 sensors were not always possible due to the impacts of cloud contaminations, topographic
722 shadows, snow cover and revisit periods (Williamson et al., 2018; Paul et al., 2020)–
723 (Williamson et al., 2018; Paul et al., 2020) (Williamson et al., 2018; Paul et al., 2020).

724 Glacial lakes are changing temporally in the context of climate and glacier changes, taking
725 supraglacial lakes for example that evolve dramatically in a short period observed between
726 Landsat and Sentinel-2 images (Figure 12eFigure 11Figure 8d). Despite our efforts of
727 leveraging all available high-quality images, the overlap of acquisition dates between Landsat
728 and Sentinel-2 images for the same location is relatively low (only 7 scenes of Sentinel-2
729 images or 112 glacial lakes in 2020) in this study area, and the consequential temporal gaps
730 led to a difference in the number and area of the derived glacial lakes.

731 ~~Displacement between images also resulted in a certain degree of discrepancy between Landsat~~
732 ~~and Sentinel derived glacial lakes. All images used in this study have been orthorectified before~~
733 ~~download, but we still find that one Sentinel image was not well matched with Landsat images,~~
734 ~~leading to the discrepancy between the two glacial lake datasets (Figure 12f). We manually~~
735 ~~georeferenced the shifted image to minimize the difference between Sentinel and Landsat~~
736 ~~derived glacial lakes (Figure 12f). Original geo-referencing accuracy is approximately half of~~
737 ~~one pixel for Landsat and Sentinel image, and this displacement likely contributes a minor error~~
738 ~~to glacial lake changes at various time periods. Although we could not eliminate this intrinsic~~
739 ~~error, the error has been considered in the uncertainty assessment of our glacial lake mapping.~~



740
741



742
743
744
745

Figure 11812. Discrepancy of lake extents extracted from Landsat and Sentinel-2 images.

746

747 An increasing number of glacier lake datasets have been released over the past years, and
 748 most of them were produced from long-term Landsat archives. Regional glacial lake datasets
 749 using Sentinel images are scarce. Lack of Sentinel-derived glacial lake data in the study area
 750 makes it impossible to compare. Here we selected four available glacial lake datasets to
 751 compare with our Landsat-derived dataset.

752 Our study provides the latest glacial lake dataset (in 2020) and the most long-term 30-m
 753 Landsat observation (1990 to 2020) for this study, with a range of critical attributes including
 754 two types of classification systems. Within the same study area, our 2020 glacial lakes appear
 755 to be closest to the 2018 dataset produced by Wang et al. (2020), with the highest overlap of
 756 greater than 74% in both number and area (\cdot). In Wang et al. (2020), the minimum mapping
 757 unit is 6 pixels so their dataset has a smaller lake quantity. However, their dataset contains
 758 many large landslide-dammed lakes that are excluded in our glacial lake mapping. As a
 759 result, their total glacier lake area is greater than ours. The overlapping rates between Wang's
 760 glacial lakes (2020) in 1990 and ours are more than 69% in both number and area. However,
 761 their results show a distinct increase of glacial lakes in number and area between 1990 and
 762 2018 (Wang et al., 2020) whereas our data show a more stable change between 1990 and
 763 2020. One possible reason is that manually delineating glacial lakes twice by different
 764 operators during Wang's lake mapping (2020) exacerbates the errors of mapping. Another
 765 reason is that their data contains landslide-dammed lakes that fluctuate greatly with time and
 766 expanded recently. One example is the Attabad Lake (Located at $36^{\circ}18'22.33''N$,
 767 $74^{\circ}49'34.36''E$).

768

769 **Table 6.** Comparison of different glacial lake datasets sourced from Landsat images in the study area.

Baseline year (period)	Method	MMU m^2 (pixels)	Count (km^2)	Overlap % (%)	Reference
1990 (1988-1993)	Manual	5400 (6)	1720 (89.68 \pm 13.69)	69.17 (76.33)	Wang et al., 2020
1990 (1990-1999)	Automated	50000 (55)	145 (20.28)	6.27 (21.66)	Shugar et al., 2020
1990 (1989-1992)	Manual	2700 (3)	622 (51.93 \pm 10.15)	27.72 (39.94)	Zhang et al., 2015
1990 (1989-1994)	Semi-automated	4500 (5)	2154 (85.10 \pm 14.66)	—	This study
2000 (1999-2001)	Manual	2700 (3)	724 (61.41 \pm 11.91)	31.91 (46.97)	Zhang et al., 2015
2000 (2000-2004)	Automated	50000 (55)	155 (22.35)	6.78 (23.72)	Shugar et al., 2020
2008	Automated & Manual	8100 (9)	1067 (65.45)	44.14 (53.58)	Chen et al., 2021
2000 (1996-2004)	Semi-automated	4500 (5)	2184 (86.10 \pm 14.83)	—	This study
2015 (2015-2018)	Automated	50000 (55)	148 (21.45)	6.27 (22.97)	Shugar et al., 2020
2017	Automated & Manual	8100 (9)	1063 (63.23)	45.21 (57.78)	Chen et al., 2021
2018 (2017-2018)	Manual	5400 (6)	1956 (102.46 \pm 15.48)	74.57 (85.63)	Wang et al., 2020
2020 (2016-2020)	Semi-automated	4500 (5)	2234 (86.31 \pm 14.98)	—	This study

770 Note: MMU represents minimum mapping units. Overlap % (%) represent the rates in count and area calculated by dividing
 771 individual glacial dataset by our Landsat-derived data in the nearest baseline year respectively.

772

773 The second highest overlapping rate is approximate 54% for 2008 and 58% for 2017 in area
 774 comparing with Chen's data (Chen et al., 2021). However, the overlapping rate in number is

775 nearly 45% due to their larger minimum mapping unit (9 pixels). Similarly, a minimum
776 mapping unit of 55 pixels (50000 m²) in Shugar et al.'s dataset (2020) led to the lowest overlap
777 with less than 24% in area. The dataset from Zhang et al. (2015) shows fewer glacial lakes in
778 1990 and 2000 even with a smaller MMU of 3 pixels. By inspecting their dataset, we attributed
779 this anomalous discrepancy to a range of glacial lakes that were missing due to lack of thorough
780 cross-check quality assurance and the limit of a 10-km buffer zone from glaciers during their
781 manual delineation. Our Landsat derived glacial lake dataset has been visually cross-checked
782 over three time periods after the step of threshold-based semiautomated lake mapping, and also
783 been visually validated by Sentinel-2 derived glacial lakes. Through this series of quality
784 assurance, we aim at delivering one of the most reliable multi-decadal glacial lake products for
785 this study area.

786 Other factors, such as minimum mapping units, definition of glacial lakes and study areas,
787 image quality and acquisition dates, mapping methods and quality assurance workflow, might
788 also lead to the discrepancies between the glacial lake datasets. Despite such discrepancies,
789 an increasing number of publically shared datasets benefit potential users to select the most-
790 suitable one for their objectives. Herein, we provide an up-to-date glacial lake dataset derived
791 from both Landsat and Sentinel observations, which further increased the availability of
792 glacial lake datasets for GLOFs risk assessment, predicting glacier evolutions cryosphere-
793 hydrological changes in the context of climate change.

794 6.3 Limitation and updating plan

795 We would like to acknowledge several limitations of our glacier lake dataset, largely due the
796 availability of high quality satellite images in the study area and inadequate field survey data
797 (Wang et al., 2020; Chen et al., 2021)(~~Wang et al., 2020; Chen et al., 2021~~)(~~Wang et al.,~~
798 ~~2020; Chen et al., 2021~~). First, it is unlikely to collect enough good-quality images within one
799 calendar year for the entire study area due to high possibility of cloud or snow covers. Even
800 though the capacity of repeat observations for Landsat-8 OLI and Sentinel-2 increased (Roy
801 et al., 2014; Williamson et al., 2018; Wulder et al., 2019; Paul et al., 2020), the 2020 glacial
802 lake dataset has to employ images acquired in adjacent other-years besides 2020. Most
803 images used from Landsat and Sentinel-2 platforms were imaged in autumn, and some
804 images taken between April and July and in November also were employed. Distribution and
805 changes in glacial lakes primarily represent the characteristics between August and October.
806 Glacial lakes evolve with time and space (Nie et al., 2017), and subtle inter- and intra-annual
807 changes (Liu et al., 2020) for each time period were ignored. Second, field investigation data
808 are limited due to low accessibility of high mountain environment in the study area, which
809 restrained the accuracy in classifying the glacial lake types. Although very high-resolution
810 Google Earth images were utilized to assist in lake type interpretation, occasional
811 misclassification was unavoidableinevitable. We implemented two types of classification
812 systems based on a careful utilization of glacier data, DEM, geomorphological features and
813 expert knowledge. However, the lack of in situ survey prohibited a thorough validation of the
814 glacial lake types. ~~Furthermore~~Third, the rigorous quality assurance and cross check after
815 semi-automated lake mapping assure the quality of our lake dataset but method we have
816 adopted isare still time and cost prohibitive~~labor-intensive~~,. State-of-the-art mapping
817 methods, such as deep learning method (Wu et al., 2020), Google Earth Engine cloud-

818 computing (Chen et al., 2021) and synergy of SAR and optical images (Wangchuk and
819 Bolch, 2020; How et al., 2021), would be used in the future to balance product accuracy and
820 time cost.

821 The glacial lake dataset will be updated using newly collected Landsat and Sentinel
822 images at a five-year interval or modified according to user feedbacks. The updated glacial
823 lake dataset will continue to be released freely and publicly on the Mountain Science Data
824 Center sharing platform.

825 **the improvement of the method will also be the direction of our future**
826 **research.**

827 **7 Data availability**

828 Our glacial lake dataset extracted from Sentinel-2 images in 2020 and Landsat observation
829 between 1990 and 2020 are available online via the Mountain Science Data Center, the
830 Institute of Mountain Hazards and Environment, the Chinese Academy of Sciences at
831 <https://doi.org/10.12380/Glaci.msdc.000001> (Lesi et al., 2022)-~~(Lesi et al., 2022)~~ (~~Lesi et al.,~~
832 ~~2022~~). The glacial lake dataset is provided in both ESRI shapefile format (total size of 22.6
833 MB) and the Geopackage format (version 1.2.1) with a total size of 9.2MB, which can be
834 opened and further processed by open-source geographic information system software such
835 as QGIS. ~~The glacial lake dataset will be updated using newly collected Landsat and Sentinel~~
836 ~~images at a five-year interval or modified according to user feedbacks. The updated glacial~~
837 ~~lake dataset will continue to be released freely and publicly on the Mountain Science Data~~
838 ~~Center sharing platform.~~

839 **8 Conclusions**

840 Glacial lake inventories of the entire China-Pakistan Economic Corridor in 2020 were
841 ~~completed provided~~ based on Landsat and Sentinel-2 images using a ~~human interactive~~
842 ~~anthreshold-based~~ semi-automated mapping method. Both Landsat and Sentinel-2 derived
843 glacial lake datasets show similar characteristics in spatial distribution and in the statistics of
844 count and area. By contrast, glacial lake dataset derived from Sentinel-2 images with a spatial
845 resolution of 10 m has a lower mapping error and more accurate lake boundary than those
846 from 30 m spatial resolution Landsat images whereas Landsat imagery is more suitable to
847 analyze spatial-temporal changes at a longer time scale due to its long-term archived
848 observations at a consistent 30 m spatial resolution ~~of 30 m~~ starting from ~~around 1990~~ the late
849 1980s.

850 Glacial lakes in the study area remain relatively stable with a slight increase in number and
851 area between 1990 and 2020 according to Landsat observations. Our dataset reveals that 2154
852 glacial lakes in 1990 covering 85.1 ± 14.66 km² increased to 2234 lakes with a total area of
853 86.31 ± 14.98 km². The same mapping method and rigorous workflow of quality assurance
854 and quality control used in this study reduced the error in multi-temporal changes of glacial
855 lakes.

856 The Hanshaw's error estimation method for pixel-based automated lake mapping was
857 improved by removing repeatedly calculated edge pixels that vary with lake shape. Therefore,
858 the newly proposed method reduces the estimated value of uncertainty from satellite
859 observations. The average relative error is $\pm 17.36\%$ for Landsat-derived product and $\pm 8.15\%$
860 for product from Sentinel-2.

861 Our glacial lake dataset contains a range of critical parameters that maximize their
862 potential utility for water resource and GLOFs risk evaluation, cryosphere-hydrological and
863 glacier-lake evolution projection. The dual classification systems of glacial lake types were
864 developed and are very likely to attract broader researchers and scientists to use our datasets.
865 In comparison with other existing glacial lake datasets, our products were created through a
866 thorough consideration of lake types, cross checks and rigorous quality assurance, and will be
867 updated and released continuously in the ~~data center of~~ Mountain Science Data Center. As
868 such, we expect that our glacial lake dataset will have significant value to cryospheric-
869 hydrology research, the assessment of water resource and glacier-related hazards ~~and~~
870 ~~engineering project construction~~ in the CPEC.

871
872 **Supplement Appendix.** The supplement appendix related to this article is available online.

873
874 **Author contributions.** ML and YN conceived the study, ML, YN and XD performed data
875 processing and analysis of the glacial lake inventory data, JW contributed to tool
876 development and mapping methods, ML and YN wrote the manuscript. All authors reviewed
877 and edited the manuscript before submission.

878
879 **Competing interests.** The authors declare no conflict of interest.

880 881 **Acknowledgements.**

882 We are grateful for the editor Kenneth Mankoff and three anonymous referees for their
883 constructive comments that greatly help us to improve this manuscript. This study was
884 supported by the second Tibetan Plateau Scientific Expedition and Research Program (grant
885 2019QZKK0603), the National Natural Science Foundation of China (Grant Nos. 42171086,
886 41971153), the International Science & Technology Cooperation Program of China (No.
887 2018YFE0100100), the Chinese Academy of Sciences "Light of West China" and Natural
888 Sciences and Engineering Research Council of Canada (Grant No. DG-2020-04207).

889
890
891 -

892 **References**

893 Ashraf, A., Naz, R., Iqbal, M.B.: Altitudinal dynamics of glacial lakes under changing climate in the Hindu
894 Kush, Karakoram, and Himalaya ranges. *Geomorphology*, 283: 72-79,
895 <https://doi.org/10.1016/j.geomorph.2017.01.033>, 2017.

896 [Azam, M.F., Kargel, J.S., Shea, J.M., Nepal, S., Haritashya, U.K., Srivastava, S., Maussion, F., Qazi, N.,](#)
897 [Chevallier, P., Dimri, A.P., Kulkarni, A.V., Cogley, J.G., Bahuguna, I.: Glaciohydrology of the Himalaya-](#)
898 [Karakoram. *Science*, 373: eabf3668, <https://doi.org/10.1126/science.abf3668>, 2021.](#)

899 [Battamo, A.Y., Varis, O., Sun, P., Yang, Y., Oba, B.T., Zhao, L.: Mapping socio-ecological resilience along the](#)
900 [seven economic corridors of the Belt and Road Initiative. *J. Clean. Prod.*, 309: 127341,](#)
901 [<https://doi.org/10.1016/j.jclepro.2021.127341>, 2021.](#)

902 [Bhambri, R., Hewitt, K., Kawishwar, P., Kumar, A., Verma, A., Snehmani, Tiwari, S., Misra, A.: Ice-dams,](#)
903 [outburst floods, and movement heterogeneity of glaciers, Karakoram. *Global Planet. Change*, 180: 100-116,](#)
904 [<https://doi.org/10.1016/j.gloplacha.2019.05.004>, 2019.](#)

905 [Bhattacharya, A., Bolch, T., Mukherjee, K., King, O., Menounos, B., Kapitsa, V., Neckel, N., Yang, W., Yao,](#)
906 [T.: High Mountain Asian glacier response to climate revealed by multi-temporal satellite observations since the](#)
907 [1960s. *Nat. Commun.*, 12: 4133, <https://doi.org/10.1038/s41467-021-24180-y>, 2021.](#)

908 [Bolch, T., Pieczonka, T., Mukherjee, K., Shea, J.: Brief communication: Glaciers in the Hunza catchment](#)
909 [\(Karakoram\) have been nearly in balance since the 1970s. *The Cryosphere*, 11: 531-539,](#)
910 [<https://doi.org/10.5194/tc-11-531-2017>, 2017.](#)

911 [Brun, F., Berthier, E., Wagnon, P., Kääh, A., Treichler, D.: A spatially resolved estimate of High Mountain Asia](#)
912 [glacier mass balances from 2000 to 2016. *Nat. Geosci.*, 10: 668-673, <https://doi.org/10.1038/ngeo2999>, 2017.](#)

913 [Brun, F., Wagnon, P., Berthier, E., Jomelli, V., Maharjan, S.B., Shrestha, F., Kraaijenbrink, P.D.A.:](#)
914 [Heterogeneous Influence of Glacier Morphology on the Mass Balance Variability in High Mountain Asia. *J.*](#)
915 [*Geophys. Res-Earth*, 124: 1331-1345, <https://doi.org/10.1029/2018JF004838>, 2019.](#)

916 [Carrivick, J.L., Tweed, F.S.: Proglacial lakes: character, behaviour and geological importance. *Quaternary Sci.*](#)
917 [*Rev.*, 78: 34-52, <https://doi.org/10.1016/j.quascirev.2013.07.028>, 2013.](#)

918 [Carrivick, J.L., Quincey, D.J.: Progressive increase in number and volume of ice-marginal lakes on the western](#)
919 [margin of the Greenland Ice Sheet. *Global Planet. Change*, 116: 156-163,](#)
920 [<https://doi.org/10.1016/j.gloplacha.2014.02.009>, 2014.](#)

921 [Carrivick, J.L., Tweed, F.S.: A global assessment of the societal impacts of glacier outburst floods. *Global*](#)
922 [*Planet. Change*, 144: 1-16, <https://doi.org/10.1016/j.gloplacha.2016.07.001>, 2016.](#)

923 [Carrivick, J.L., Tweed, F.S., Sutherland, J.L., Mallalieu, J.: Toward Numerical Modeling of Interactions](#)
924 [Between Ice-Marginal Proglacial Lakes and Glaciers. *Front. Earth Sci*, 8,](#)
925 [<https://doi.org/10.3389/feart.2020.577068>, 2020.](#)

926 [Carrivick, J.L., How, P., Lea, J.M., Sutherland, J.L., Grimes, M., Tweed, F.S., Cornford, S., Quincey, D.J.,](#)
927 [Mallalieu, J.: Ice-Marginal Proglacial Lakes Across Greenland: Present Status and a Possible Future. *Geophys.*](#)
928 [*Res. Lett.*, 49: e2022GL099276, <https://doi.org/https://doi.org/10.1029/2022GL099276>, 2022.](#)

929 [Chen, F., Zhang, M., Guo, H., Allen, S., Kargel, J.S., Haritashya, U.K., Watson, C.S.: Annual 30 m dataset for](#)
930 [glacial lakes in High Mountain Asia from 2008 to 2017. *Earth System Science Data*, 13: 741-766,](#)
931 [<https://doi.org/10.5194/essd-13-741-2021>, 2021.](#)

932 [Chen, X., Cui, P., You, Y., Cheng, Z., Khan, A., Ye, C., Zhang, S.: Dam-break risk analysis of the Attabad](#)
933 [landslide dam in Pakistan and emergency countermeasures. *Landslides*, 14: 675-683,](#)
934 [<https://doi.org/10.1007/s10346-016-0721-7>, 2017.](#)

935 [Cook, S.J., Quincey, D.J.: Estimating the volume of Alpine glacial lakes. *Earth Surf. Dynam.*, 3: 559-575,](#)
936 [<https://doi.org/10.5194/esurf-3-559-2015>, 2015.](#)

937 [Emmer, A., Cuřín, V.: Can a dam type of an alpine lake be derived from lake geometry? A negative result. *J.*](#)
938 [*Mt. Sci.-Engl.*, 18: 614-621, <https://doi.org/10.1007/s11629-020-6003-9>, 2021.](#)

939 [Farr, T.G., Rosen, P.A., Caro, E., Crippen, R., Duren, R., Hensley, S., Kobrick, M., Paller, M., Rodriguez, E.,](#)

940 [Roth, L., Seal, D., Shaffer, S., Shimada, J., Umland, J., Werner, M., Oskin, M., Burbank, D., Alsdorf, D.: The](#)
941 [Shuttle Radar Topography Mission. Rev. Geophys., 45: RG2004, <https://doi.org/10.1029/2005RG000183>, 2007.](#)
942 [Gardelle, J., Arnaud, Y., Berthier, E.: Contrasted evolution of glacial lakes along the Hindu Kush Himalaya](#)
943 [mountain range between 1990 and 2009. Global Planet. Change, 75: 47-55,](#)
944 [<https://doi.org/10.1016/j.gloplacha.2010.10.003>, 2011.](#)
945 [Hanshaw, M.N., Bookhagen, B.: Glacial areas, lake areas, and snow lines from 1975 to 2012: status of the](#)
946 [Cordillera Vilcanota, including the Quelccaya Ice Cap, northern central Andes, Peru. The Cryosphere, 8: 359-](#)
947 [376, <https://doi.org/10.5194/tc-8-359-2014>, 2014.](#)
948 [Hewitt, K.: The Karakoram Anomaly? Glacier Expansion and the 'Elevation Effect,' Karakoram Himalaya. Mt.](#)
949 [Res. Dev., 25: 332-340, \[https://doi.org/10.1659/0276-4741\\(2005\\)025\\[0332:TKAGEA\\]2.0.CO;2\]\(https://doi.org/10.1659/0276-4741\(2005\)025\[0332:TKAGEA\]2.0.CO;2\), 2005.](#)
950 [Hewitt, K., 2014. Glaciers of the Karakoram Himalaya: Glacial Environments, Processes, Hazards and](#)
951 [Resources. Springer, Dordrecht.](#)
952 [How, P., Messerli, A., Mätzler, E., Santoro, M., Wiesmann, A., Caduff, R., Langley, K., Bojesen, M.H., Paul,](#)
953 [F., Kääh, A., Carrivick, J.L.: Greenland-wide inventory of ice marginal lakes using a multi-method approach.](#)
954 [Sci. Rep.-UK, 11: 4481, <https://doi.org/10.1038/s41598-021-83509-1>, 2021.](#)
955 [Huggel, C., Kääh, A., Haerberli, W., Teyssere, P., Paul, F.: Remote sensing based assessment of hazards from](#)
956 [glacier lake outbursts: a case study in the Swiss Alps. Can. Geotech. J., 39: 316-330,](#)
957 [<https://doi.org/10.1139/t01-099>, 2002.](#)
958 [Hugonnet, R., McNabb, R., Berthier, E., Menounos, B., Nuth, C., Girod, L., Farinotti, D., Huss, M., Dussaillant,](#)
959 [I., Brun, F., Kääh, A.: Accelerated global glacier mass loss in the early twenty-first century. Nature, 592: 726-](#)
960 [731, <https://doi.org/10.1038/s41586-021-03436-z>, 2021.](#)
961 [Huss, M., Hock, R.: Global-scale hydrological response to future glacier mass loss. Nat. Clim. Change, 8: 135-](#)

962 [140, https://doi.org/10.1038/s41558-017-0049-x](https://doi.org/10.1038/s41558-017-0049-x), 2018.

963 [Immerzeel, W.W., Lutz, A.F., Andrade, M., Bahl, A., Biemans, H., Bolch, T., Hyde, S., Brumby, S., Davies,](#)

964 [B.J., Elmore, A.C., Emmer, A., Feng, M., Fernández, A., Haritashya, U., Kargel, J.S., Koppes, M.,](#)

965 [Kraaijenbrink, P.D.A., Kulkarni, A.V., Mayewski, P.A., Nepal, S., Pacheco, P., Painter, T.H., Pellicciotti, F.,](#)

966 [Rajaram, H., Rupper, S., Sinisalo, A., Shrestha, A.B., Viviroli, D., Wada, Y., Xiao, C., Yao, T., Baillie, J.E.M.:](#)

967 [Importance and vulnerability of the world's water towers. Nature, 577: 364-369, https://doi.org/10.1038/s41586-](#)

968 [019-1822-y, 2020.](#)

969 [Jarvis, A., Reuter, H.I., Nelson, A., Guevara, E., 2008. Hole-filled seamless SRTM data V4. 2008, International](#)

970 [Centre for Tropical Agriculture \(CIAT\), available from <http://srtm.csi.cgiar.org>.](#)

971 [Jiang, S., Nie, Y., Liu, Q., Wang, J., Liu, L., Hassan, J., Liu, X., Xu, X.: Glacier Change, Supraglacial Debris](#)

972 [Expansion and Glacial Lake Evolution in the Gyirong River Basin, Central Himalayas, between 1988 and 2015.](#)

973 [Remote Sens.-Basel, 10: 986, https://doi.org/10.3390/rs10070986, 2018.](#)

974 [Kääb, A., Berthier, E., Nuth, C., Gardelle, J., Arnaud, Y.: Contrasting patterns of early twenty-first-century](#)

975 [glacier mass change in the Himalayas. Nature, 488: 495-498, https://doi.org/10.1038/nature11324, 2012.](#)

976 [Lesi, M., Nie, Y., Shugar, D.H., Wang, J., Deng, Q., Chen, H.: Landsat and Sentinel-derived glacial lake dataset](#)

977 [in the China-Pakistan Economic Corridor from 1990 to 2020. Mountain Science Data Center,](#)

978 [https://doi.org/10.12380/Glaci.msdc.000001 CSTR:1a006.11.Glaci.msdc.000001, 2022.](#)

979 [Li, D., Shangguan, D., Anjum, M.N.: Glacial Lake Inventory Derived from Landsat 8 OLI in 2016–2018 in](#)

980 [China–Pakistan Economic Corridor. ISPRS international journal of geo-information, 9: 294,](#)

981 [https://doi.org/10.3390/ijgi9050294, 2020.](#)

982 [Li, Z., Deng, X., Zhang, Y.: Evaluation and convergence analysis of socio-economic vulnerability to natural](#)

983 [hazards of Belt and Road Initiative countries. J. Clean. Prod., 282: 125406,](#)

984 <https://doi.org/10.1016/j.jclepro.2020.125406>, 2021.

985 [Liu, Q., Mayer, C.: Distribution and interannual variability of supraglacial lakes on debris-covered glaciers in](#)
986 [the Khan Tengri-Tumor Mountains, Central Asia. Environ. Res. Lett., 10: 014014 2015.](#)

987 [Liu, Q., Mayer, C., Wang, X., Nie, Y., Wu, K., Wei, J., Liu, S.: Interannual flow dynamics driven by frontal](#)
988 [retreat of a lake-terminating glacier in the Chinese Central Himalaya. Earth Planet. Sc. Lett., 546: 116450,](#)
989 <https://doi.org/10.1016/j.epsl.2020.116450>, 2020.

990 [Lyons, E.A., Sheng, Y., Smith, L.C., Li, J., Hinkel, K.M., Lenters, J.D., Wang, J.: Quantifying sources of error](#)
991 [in multitemporal multisensor lake mapping. Int. J. Remote Sens., 34: 7887-7905,](#)
992 <https://doi.org/10.1080/01431161.2013.827343>, 2013.

993 [Mankoff, K.D., Noël, B., Fettweis, X., Ahlstrøm, A.P., Colgan, W., Kondo, K., Langley, K., Sugiyama, S., van](#)
994 [As, D., Fausto, R.S.: Greenland liquid water discharge from 1958 through 2019. Earth Syst. Sci. Data, 12: 2811-](#)
995 [2841, https://doi.org/10.5194/essd-12-2811-2020](#), 2020.

996 [Martín, C.N.S., Ponce, J.F., Montes, A., Balocchi, L.D., Gorza, C., Andrea, C.: Proglacial landform assemblage](#)
997 [in a rapidly retreating cirque glacier due to temperature increase since 1970, Fuegian Andes, Argentina.](#)
998 [Geomorphology, 390: 107861, https://doi.org/10.1016/j.geomorph.2021.107861](#), 2021.

999 [Maurer, J.M., Schaefer, J.M., Rupper, S., Corley, A.: Acceleration of ice loss across the Himalayas over the past](#)
1000 [40 years. Sci. Adv., 5: eaav7266, https://doi.org/10.1126/sciadv.aav7266](#), 2019.

1001 [Mcfeters, S.K.: The use of the Normalized Difference Water Index \(NDWI\) in the delineation of open water](#)
1002 [features. Int. J. Remote Sens., 17: 1425 - 1432 1996.](#)

1003 [Miles, E.S., Watson, C.S., Brun, F., Berthier, E., Esteves, M., Quincey, D.J., Miles, K.E., Hubbard, B., Wagon,](#)
1004 [P.: Glacial and geomorphic effects of a supraglacial lake drainage and outburst event, Everest region, Nepal](#)
1005 [Himalaya. The Cryosphere, 12: 3891-3905, https://doi.org/10.5194/tc-12-3891-2018](#), 2018.

1006 [Nie, Y., Zhang, Y., Liu, L., Zhang, J.: Glacial change in the vicinity of Mt. Qomolangma \(Everest\), central high](#)
1007 [Himalayas since 1976. J. Geogr. Sci., 20: 667-686, <https://doi.org/10.1007/s11442-010-0803-8>, 2010.](#)

1008 [Nie, Y., Sheng, Y., Liu, Q., Liu, L., Liu, S., Zhang, Y., Song, C.: A regional-scale assessment of Himalayan](#)
1009 [glacial lake changes using satellite observations from 1990 to 2015. Remote Sens. Environ., 189: 1-13,](#)
1010 [<https://doi.org/10.1016/j.rse.2016.11.008>, 2017.](#)

1011 [Nie, Y., Liu, Q., Wang, J., Zhang, Y., Sheng, Y., Liu, S.: An inventory of historical glacial lake outburst floods](#)
1012 [in the Himalayas based on remote sensing observations and geomorphological analysis. Geomorphology, 308:](#)
1013 [91-106, <https://doi.org/10.1016/j.geomorph.2018.02.002>, 2018.](#)

1014 [Nie, Y., Liu, W., Liu, Q., Hu, X., Westoby, M.J.: Reconstructing the Chongbaxia Tsho glacial lake outburst](#)
1015 [flood in the Eastern Himalaya: Evolution, process and impacts. Geomorphology, 370: 107393,](#)
1016 [<https://doi.org/10.1016/j.geomorph.2020.107393>, 2020.](#)

1017 [Nie, Y., Pritchard, H.D., Liu, Q., Hennig, T., Wang, W., Wang, X., Liu, S., Nepal, S., Samyn, D., Hewitt, K.,](#)
1018 [Chen, X.: Glacial change and hydrological implications in the Himalaya and Karakoram. Nature Reviews Earth](#)
1019 [& Environment, 2: 91-106, <https://doi.org/10.1038/s43017-020-00124-w>, 2021.](#)

1020 [Paul, F., Rastner, P., Azzoni, R.S., Diolaiuti, G., Fugazza, D., Le Bris, R., Nemec, J., Rabatel, A., Ramusovic,](#)
1021 [M., Schwaizer, G., Smiraglia, C.: Glacier shrinkage in the Alps continues unabated as revealed by a new glacier](#)
1022 [inventory from Sentinel-2. Earth System Science Data, 12: 1805-1821, \[https://doi.org/10.5194/essd-12-1805-\]\(https://doi.org/10.5194/essd-12-1805-2020\)](#)
1023 [2020, 2020.](#)

1024 [Pfeffer, W.T., Arendt, A.A., Bliss, A., Bolch, T., Cogley, J.G., Gardner, A.S., Hagen, J., Hock, R., Kaser, G.,](#)
1025 [Kienholz, C., Miles, E.S., Moholdt, G., Mölg, N., Paul, F., Radić, V., Rastner, P., Raup, B.H., Rich, J., Sharp,](#)
1026 [M.J.: The Randolph Glacier Inventory: a globally complete inventory of glaciers. J. Glaciol., 60: 537-552,](#)
1027 [<https://doi.org/10.3189/2014JoG13J176>, 2014.](#)

1028 [Post, A., Mayo, L.R., 1971. Glacier dammed lakes and outburst floods in Alaska: U.S. Geological Survey](#)

1029 [Hydrologic Investigations Atlas 455, U.S. Geological Survey.](#)

1030 [Pritchard, H.D.: Asia's shrinking glaciers protect large populations from drought stress. Nature, 569: 649-654,](#)

1031 [https://doi.org/10.1038/s41586-019-1240-1, 2019.](https://doi.org/10.1038/s41586-019-1240-1)

1032 [Quincey, D.J., Richardson, S.D., Luckman, A., Lucas, R.M., Reynolds, J.M., Hambrey, M.J., Glasser, N.F.:](#)

1033 [Early recognition of glacial lake hazards in the Himalaya using remote sensing datasets. Global Planet. Change,](#)

1034 [56: 137-152, https://doi.org/10.1016/j.gloplacha.2006.07.013, 2007.](#)

1035 [Rabus, B., Eineder, M., Roth, A., Bamler, R.: The shuttle radar topography mission—a new class of digital](#)

1036 [elevation models acquired by spaceborne radar. ISPRS J. Photogramm., 57: 241-262,](#)

1037 [https://doi.org/10.1016/S0924-2716\(02\)00124-7, 2003.](https://doi.org/10.1016/S0924-2716(02)00124-7)

1038 [RGI Consortium: Randolph Glacier Inventory – A Dataset of Global Glacier Outlines: Version 6.0: Technical](#)

1039 [Report, https://doi.org/10.7265/N5-RGI-60, 2017.](#)

1040 [Rick, B., Mcgrath, D., Armstrong, W., Mccoy, S.W.: Dam type and lake location characterize ice-marginal lake](#)

1041 [area change in Alaska and NW Canada between 1984 and 2019. The Cryosphere, 16: 297-314,](#)

1042 [https://doi.org/10.5194/tc-16-297-2022, 2022.](https://doi.org/10.5194/tc-16-297-2022)

1043 [Rose, A., Mckee, J., Sims, K., Bright, E., Reith, A., Urban, M.: LandScan Global 2020,](#)

1044 [https://doi.org/https://doi.org/10.48690/1523378, 2021.](https://doi.org/https://doi.org/10.48690/1523378)

1045 [Rounce, D.R., Hock, R., Shean, D.E.: Glacier Mass Change in High Mountain Asia Through 2100 Using the](#)

1046 [Open-Source Python Glacier Evolution Model \(PyGEM\). Front. Earth Sci, 7: 331,](#)

1047 [https://doi.org/10.3389/feart.2019.00331, 2020.](https://doi.org/10.3389/feart.2019.00331)

1048 [Roy, D.P., Wulder, M.A., Loveland, T.R., C. E., W., Allen, R.G., Anderson, M.C., Helder, D., Irons, J.R.,](#)

1049 [Johnson, D.M., Kennedy, R., Scambos, T.A., Schaaf, C.B., Schott, J.R., Sheng, Y., Vermote, E.F., Belward,](#)

1050 [A.S., Bindschadler, R., Cohen, W.B., Gao, F., Hipple, J.D., Hostert, P., Huntington, J., Justice, C.O., Kilic, A.,](#)
1051 [Kovalskyy, V., Lee, Z.P., Lymburner, L., Masek, J.G., Mccorkel, J., Shuai, Y., Trezza, R., Vogelmann, J.,](#)
1052 [Wynne, R.H., Zhu, Z.: Landsat-8: Science and product vision for terrestrial global change research. Remote](#)
1053 [Sens. Environ., 145: 154-172, <https://doi.org/10.1016/j.rse.2014.02.001>, 2014.](#)
1054 [Sakai, A.: Brief communication: Updated GAMDAM glacier inventory over high-mountain Asia. The](#)
1055 [Cryosphere, 13: 2043-2049, <https://doi.org/10.5194/tc-13-2043-2019>, 2019.](#)
1056 [Salerno, F., Thakuri, S., D'Agata, C., Smiraglia, C., Manfredi, E.C., Viviano, G., Tartari, G.: Glacial lake](#)
1057 [distribution in the Mount Everest region: Uncertainty of measurement and conditions of formation. Global](#)
1058 [Planet. Change, 92-93: 30-39 2012.](#)
1059 [Shean, D.E., Bhushan, S., Montesano, P., Rounce, D.R., Arendt, A., Osmanoglu, B.: A Systematic, Regional](#)
1060 [Assessment of High Mountain Asia Glacier Mass Balance. Front. Earth Sci, 7: 363,](#)
1061 <https://doi.org/10.3389/feart.2019.00363>, 2020.
1062 [Sheng, Y., Song, C., Wang, J., Lyons, E.A., Knox, B.R., Cox, J.S., Gao, F.: Representative lake water extent](#)
1063 [mapping at continental scales using multi-temporal Landsat-8 imagery. Remote Sens. Environ., 185: 129-141,](#)
1064 <https://doi.org/10.1016/j.rse.2015.12.041>, 2016.
1065 [Shugar, D.H., Burr, A., Haritashya, U.K., Kargel, J.S., Watson, C.S., Kennedy, M.C., Bevington, A.R., Betts,](#)
1066 [R.A., Harrison, S., Strattman, K.: Rapid worldwide growth of glacial lakes since 1990. Nat. Clim. Change, 10:](#)
1067 [939-945, <https://doi.org/10.1038/s41558-020-0855-4>, 2020.](#)
1068 [Shugar, D.H., Jacquemart, M., Shean, D., Bhushan, S., Upadhyay, K., Sattar, A., Schwanghart, W., McBride, S.,](#)
1069 [de Vries, M., Mergili, M., Emmer, A., Deschamps-Berger, C., McDonnell, M., Bhambri, R., Allen, S., Berthier,](#)
1070 [E., Carrivick, J.L., Clague, J.J., Dokukin, M., Dunning, S.A., Frey, H., Gascoïn, S., Haritashya, U.K., Huggel,](#)
1071 [C., Kaab, A., Kargel, J.S., Kavanaugh, J.L., Lacroix, P., Petley, D., Rupper, S., Azam, M.F., Cook, S.J., Dimri,](#)

1072 [A.P., Eriksson, M., Farinotti, D., Fiddes, J., Gnyawali, K.R., Harrison, S., Jha, M., Koppes, M., Kumar, A.,](#)
1073 [Leinss, S., Majeed, U., Mal, S., Muhuri, A., Noetzli, J., Paul, F., Rashid, I., Sain, K., Steiner, J., Ugalde, F.,](#)
1074 [Watson, C.S., Westoby, M.J.: A massive rock and ice avalanche caused the 2021 disaster at Chamoli, Indian](#)
1075 [Himalaya. *Science*, 373: 300-306, <https://doi.org/10.1126/science.abh4455>, 2021.](#)
1076 [Ullah, S., You, Q., Ali, A., Ullah, W., Jan, M.A., Zhang, Y., Xie, W., Xie, X.: Observed changes in maximum](#)
1077 [and minimum temperatures over China- Pakistan economic corridor during 1980–2016. *Atmos. Res.*, 216: 37-](#)
1078 [51, <https://doi.org/10.1016/j.atmosres.2018.09.020>, 2019.](#)
1079 [Viviroli, D., Kummu, M., Meybeck, M., Kallio, M., Wada, Y.: Increasing dependence of lowland populations](#)
1080 [on mountain water resources. *Nature Sustainability*, 3: 917-928, <https://doi.org/10.1038/s41893-020-0559-9>,](#)
1081 [2020.](#)
1082 [Wang, J., Sheng, Y., Tong, T.S.D.: Monitoring decadal lake dynamics across the Yangtze Basin downstream of](#)
1083 [Three Gorges Dam. *Remote Sens. Environ.*, 152: 251-269, <https://doi.org/10.1016/j.rse.2014.06.004>, 2014.](#)
1084 [Wang, J., Sheng, Y., Wada, Y.: Little impact of the Three Gorges Dam on recent decadal lake decline across](#)
1085 [China's Yangtze Plain. *Water Resour. Res.*, 53: 3854-3877, <https://doi.org/10.1002/2016WR019817>, 2017.](#)
1086 [Wang, J., Song, C., Reager, J.T., Yao, F., Famiglietti, J.S., Sheng, Y., Macdonald, G.M., Brun, F., Schmied,](#)
1087 [H.M., Marston, R.A., Wada, Y.: Recent global decline in endorheic basin water storages. *Nat. Geosci.*, 11: 926-](#)
1088 [932, <https://doi.org/10.1038/s41561-018-0265-7>, 2018.](#)
1089 [Wang, X., Ding, Y., Liu, S., Jiang, L., Wu, K., Jiang, Z., Guo, W.: Changes of glacial lakes and implications in](#)
1090 [Tian Shan, Central Asia, based on remote sensing data from 1990 to 2010. *Environ. Res. Lett.*, 8: 44052,](#)
1091 [<https://doi.org/10.1088/1748-9326/8/4/044052>, 2013.](#)
1092 [Wang, X., Liu, S., Zhang, J.: A new look at roles of the cryosphere in sustainable development. *Advances in*](#)
1093 [*Climate Change Research*, 10: 124-131, <https://doi.org/10.1016/j.accre.2019.06.005>, 2019.](#)

1094 [Wang, X., Guo, X., Yang, C., Liu, Q., Wei, J., Zhang, Y., Liu, S., Zhang, Y., Jiang, Z., Tang, Z.: Glacial lake](#)
1095 [inventory of high-mountain Asia in 1990 and 2018 derived from Landsat images. Earth System Science Data,](#)
1096 [12: 2169-2182, <https://doi.org/10.5194/essd-12-2169-2020>, 2020.](#)

1097 [Wangchuk, S., Bolch, T.: Mapping of glacial lakes using Sentinel-1 and Sentinel-2 data and a random forest](#)
1098 [classifier: Strengths and challenges. Science of Remote Sensing, 2: 100008,](#)
1099 [<https://doi.org/https://doi.org/10.1016/j.srs.2020.100008>, 2020.](#)

1100 [Westoby, M.J., Glasser, N.F., Brasington, J., Hambrey, M.J., Quincey, D.J., Reynolds, J.M.: Modelling outburst](#)
1101 [floods from moraine-dammed glacial lakes. Earth-Sci. Rev., 134: 137-159,](#)
1102 [<https://doi.org/10.1016/j.earscirev.2014.03.009>, 2014.](#)

1103 [Williamson, A.G., Banwell, A.F., Willis, I.C., Arnold, N.S.: Dual-satellite \(Sentinel-2 and Landsat 8\) remote](#)
1104 [sensing of supraglacial lakes in Greenland. The Cryosphere, 12: 3045-3065, \[https://doi.org/10.5194/tc-12-3045-\]\(https://doi.org/10.5194/tc-12-3045-2018\)](#)
1105 [2018, 2018.](#)

1106 [Wu, R., Liu, G., Zhang, R., Wang, X., Li, Y., Zhang, B., Cai, J., Xiang, W.: A Deep Learning Method for](#)
1107 [Mapping Glacial Lakes from the Combined Use of Synthetic-Aperture Radar and Optical Satellite Images.](#)
1108 [Remote Sens.-Basel, 12: 4020](#)
1109 [2020.](#)

1110 [Wulder, M.A., Loveland, T.R., Roy, D.P., Crawford, C.J., Masek, J.G., Woodcock, C.E., Allen, R.G.,](#)
1111 [Anderson, M.C., Belward, A.S., Cohen, W.B., Dwyer, J., Erb, A., Gao, F., Griffiths, P., Helder, D., Hermosilla,](#)
1112 [T., Hipple, J.D., Hostert, P., Hughes, M.J., Huntington, J., Johnson, D.M., Kennedy, R., Kilic, A., Li, Z.,](#)
1113 [Lymburner, L., Mccorkel, J., Pahlevan, N., Scambos, T.A., Schaaf, C., Schott, J.R., Sheng, Y., Storey, J.,](#)
1114 [Vermote, E., Vogelmann, J., White, J.C., Wynne, R.H., Zhu, Z.: Current status of Landsat program, science, and](#)
1115 [applications. Remote Sens. Environ., 225: 127-147, <https://doi.org/https://doi.org/10.1016/j.rse.2019.02.015>,](#)

1116 [2019.](#)

1117 [Yao, C., Wang, X., Zhao, X., Wei, J., Zhang, Y.: Temporal and Spatial Changes of Glacial Lakes in the China-](#)

1118 [Pakistan Economic Corridor from 1990 to 2018. Journal of Glaciology and Geocryology, 42: 33-42.](#)

1119 <https://doi.org/https://doi.org/10.7522/j.issn.1000-0240.2020.0009>, 2020.

1120 [Yao, T., Thompson, L., Yang, W., Yu, W.S., Gao, Y., Guo, X.J., Yang, X.X., Duan, K.Q., Zhao, H.B., Xu,](#)

1121 [B.Q., Pu, J.C., Lu, A.X., Xiang, Y., Kattel, D.B., Joswiak, D.: Different glacier status with atmospheric](#)

1122 [circulations in Tibetan Plateau and surroundings. Nat. Clim. Change, 2: 663-667.](#)

1123 <https://doi.org/10.1038/NCLIMATE1580>, 2012.

1124 [Yao, X., Liu, S., Han, L., Sun, M., Zhao, L.: Definition and classification system of glacial lake for inventory](#)

1125 [and hazards study. J. Geogr. Sci., 28: 193-205. https://doi.org/10.1007/s11442-018-1467-z](#), 2018.

1126 [Zhang, G., Yao, T., Xie, H., Wang, W., Yang, W.: An inventory of glacial lakes in the Third Pole region and](#)

1127 [their changes in response to global warming. Global Planet. Change, 131: 148-157,](#)

1128 <https://doi.org/10.1016/j.gloplacha.2015.05.013>, 2015.

1129 [Zhang, M., Chen, F., Tian, B.: An automated method for glacial lake mapping in High Mountain Asia using](#)

1130 [Landsat 8 imagery. J. Mt. Sci.-Engl., 15: 13-24. https://doi.org/10.1007/s11629-017-4518-5](#), 2018.

1131 [Zhao, W., Xiong, D., Wen, F., Wang, X.: Lake area monitoring based on land surface temperature in the Tibetan](#)

1132 [Plateau from 2000 to 2018. Environ. Res. Lett., 15, https://doi.org/10.1088/1748-9326/ab9b41](#), 2020.

1133 [Zheng, G., Allen, S.K., Bao, A., Ballesteros-Cánovas, J.A., Huss, M., Zhang, G., Li, J., Yuan, Y., Jiang, L., Yu,](#)

1134 [T., Chen, W., Stoffel, M.: Increasing risk of glacial lake outburst floods from future Third Pole deglaciation.](#)

1135 [Nat. Clim. Change, 11: 411-417, https://doi.org/10.1038/s41558-021-01028-3](#), 2021.

1136

1137

1138 **Appendix**

1139 **Tutorial for Improved Uncertainty Estimating Method**

1140
1141 The Hanshaw’s equation was originally proposed for pixelated polygons (such as a polygon
1142 directly extracted from a remote sensing image), and performed more robustly than manually
1143 digitized polygons (where vertices do not necessarily follow the pixel edges). Our improved
1144 method also performs better for pixelated polygons. This tutorial is dedicated to helping
1145 implement our improved uncertainty estimation method.

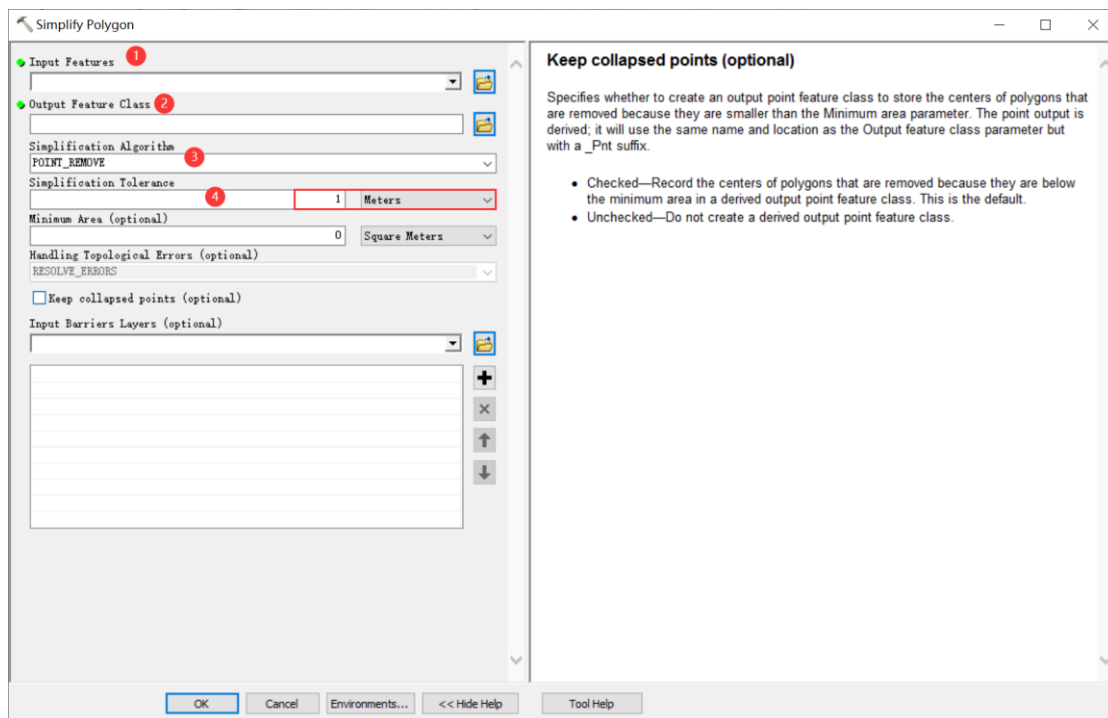
1146
1147 **Procedure of uncertainty estimating method (using ArcGIS (© ESRI) for example)**

1148 1. Removing redundant nodes (optional)

1149 We found that a small proportion (~1%) of the pixelated lake polygons (directly extracted
1150 from satellite images) have redundant nodes, which affects the value of inner nodes. If no
1151 redundant nodes exist, this step can be skipped. Or, we recommend using the “Simplify
1152 Polygon” tool in ArcGIS to remove those nodes (Figure A1Figure A1Figure A1).

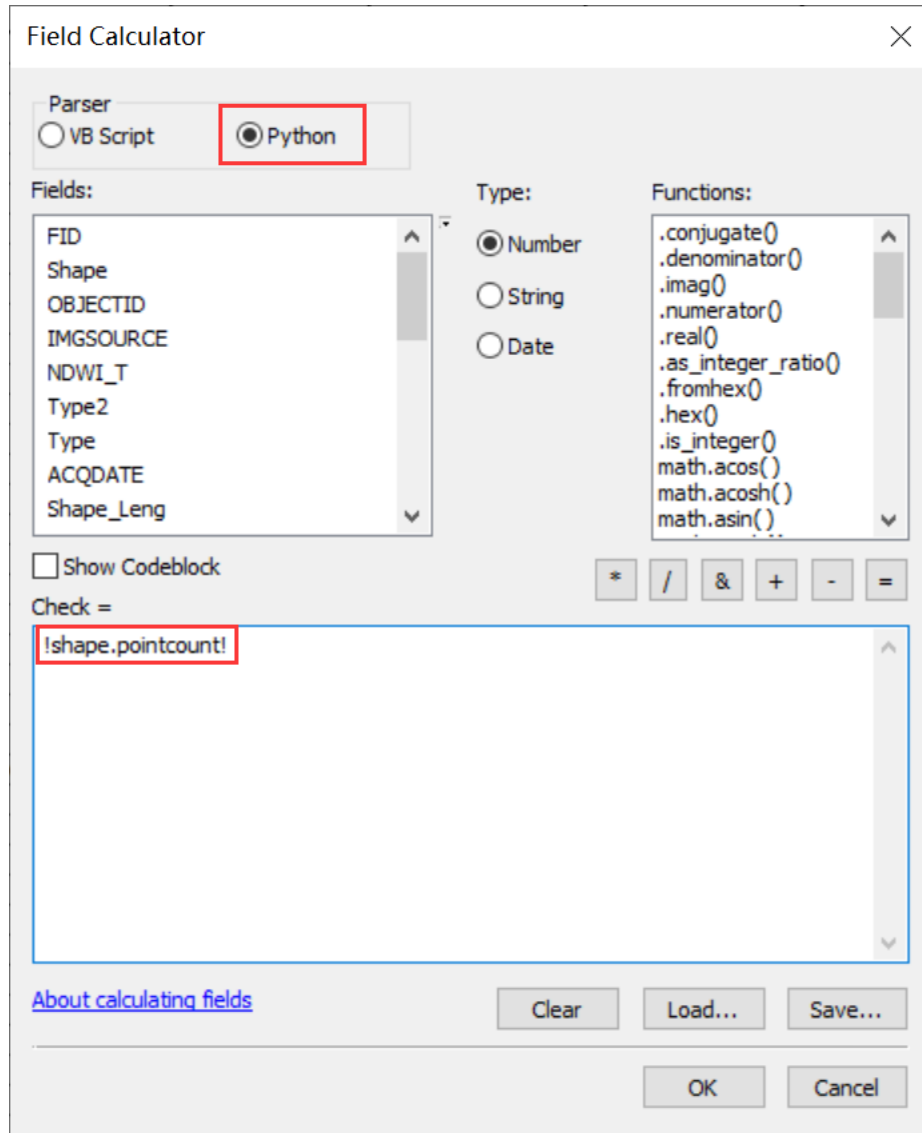
1153 In the Simplify Polygon panel

- 1154 • Input your dataset.
- 1155 • Set the output path and output file name.
- 1156 • Choose the simplification algorithm. We recommended “POINT_REMOVE”.
- 1157 • Set the tolerance of simplification algorithm. In this step, we need to ensure that the
1158 polygon boundaries remain unchanged after deleting redundant nodes. Generally, a
1159 tolerance of 1 meter will suffice, or you can adjust the threshold until your satisfaction.



1160
1161 **Figure A111.** Input and option for Simplify Polygon in ArcGIS.
1162

- 1163 2. Calculating the total number of nodes using ArcGIS (Figure A2Figure A2Figure A2):
 1164 • Add a new field in the attribute table of dataset.
 1165 • Open Field Calculator.
 1166 • Switch the parser to python mode, and enter the following code “!shape.pointcount!” in
 1167 the blue box to calculate the total number of nodes for each glacial lake boundary.

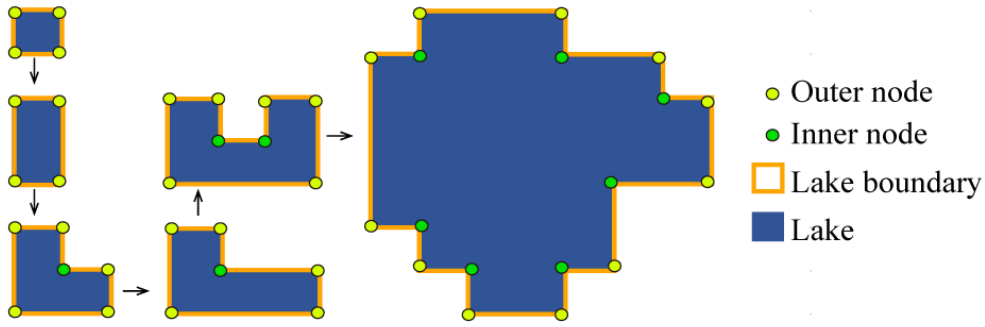


1168
 1169 **Figure A222.** Total node calculation in ArcGIS.
 1170

- 1171 3. Calculating the number of inner nodes:
 1172

1173 For polygons without islands (Figure A3Figure A3Figure A3), use the equation 5. An inner
 1174 node is a polygon vertex where the interior angle surrounding it is greater than 180 degrees.
 1175 An outer node is the opposite of the inner node, where the interior angle is less than 180
 1176 degrees. We found that the outer nodes are usually four more than the inner nodes in our
 1177 glacial lake dataset. The total nodes in ArcGIS contain one overlapping node to close the
 1178 polygon, meaning the endpoint is also the startpoint. This extra count was deleted in the
 1179 calculation (equation 5).

1180



1181

1182

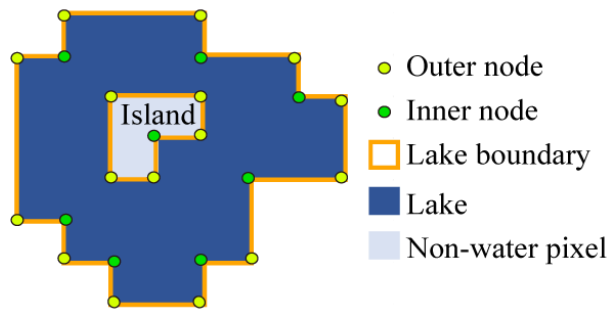
Figure A333. Sketch of outer and inner nodes of various glacial lakes without island.

1183

1184

For polygons with island (Figure A444) use the equation 6.

1185



1186

1187

Figure A444. Sketch of outer and inner nodes for glacial lake with island.

1188

1189

We further specify the steps below to help implement equation 6.

1190

1191

Sept 1: detect the number of islands within each polygon.

1192

- Convert the initial lake polygon to polyline using the “Feature To Line” tool (Figure A555).

1193

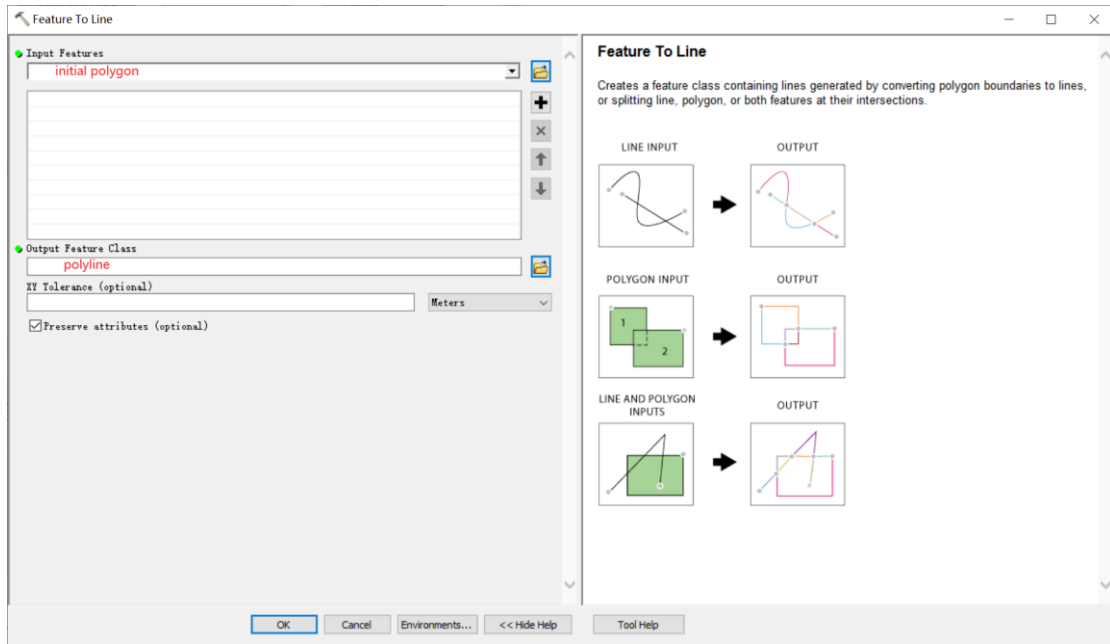


Figure A555. Feature To Line tool in ArcGIS

1194
1195
1196
1197

- Convert the polyline to generate a new polygon ([Figure A6](#)[Figure A6](#)[Figure A6](#)).

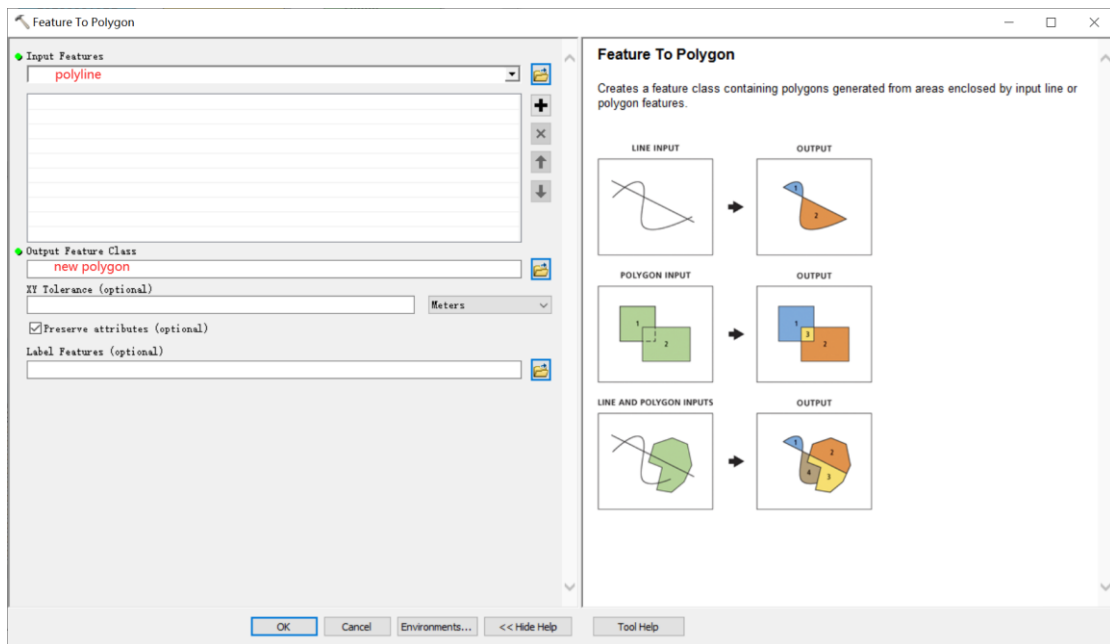


Figure A666. Feature To Polygon tool in ArcGIS

1198
1199
1200
1201
1202

- Erase the new polygon by the initial polygon, which outputs the islands. Then we can count how many islands there are in each lake ([Figure A7](#)[Figure A7](#)[Figure A7](#)).

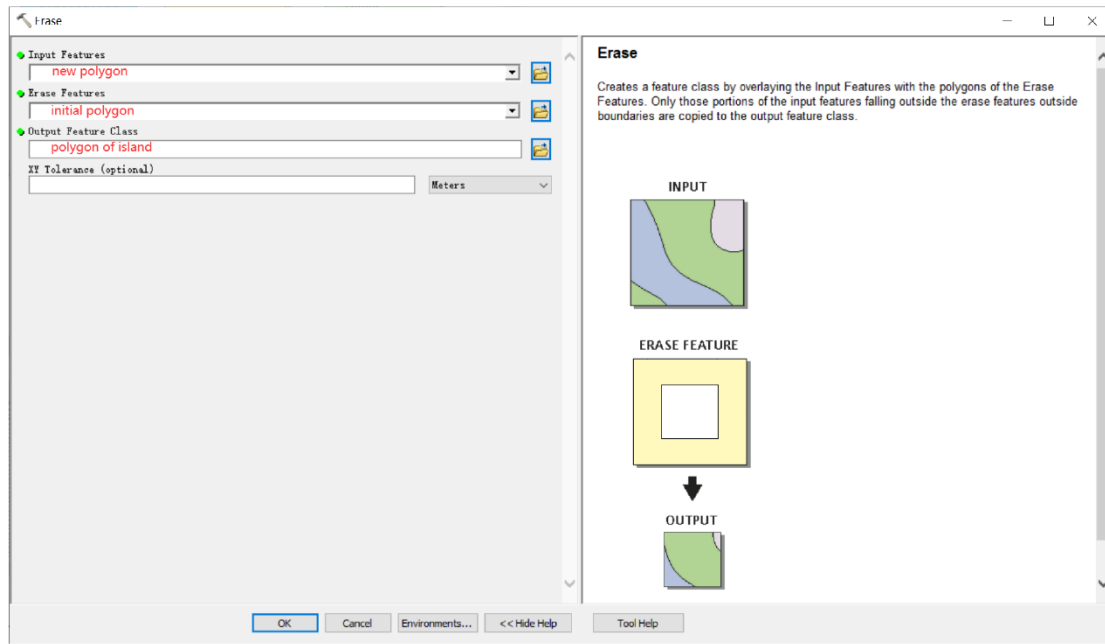


Figure A.777. Erase tool in ArcGIS.

1203
 1204
 1205
 1206
 1207
 1208
 1209

- Step 2: calculate the number of inner nodes for each polygon with island using equation 6.
4. Calculating the uncertainty of lake mapping using equation 4.